# Electrophysiology and Morphology of Human Cortical Supragranular Pyramidal Cells in a Wide Age Range

Pál Barzó[1†], Ildikó Szöts[2†], Martin Tóth[2], Éva Adrienn Csajbók[2], Gábor Molnár[2*], Gábor Tamás[2*]

[1]Department of Neurosurgery, University of Szeged, Szeged, Hungary

[2]HUN-REN-SZTE Research Group for Cortical Microcircuits, Department of Physiology, Anatomy and Neuroscience, University of Szeged, Szeged, Hungary

[†]: These authors contributed equally.
*: Equal contribution of senior authors, correspondence: gtamas@bio.u-szeged.hu

**Abstract**

The basic excitatory neurons of the cerebral cortex, the pyramidal cells, are the most important signal integrators for the local circuit. They have quite characteristic morphological and electrophysiological properties that are known to be largely constant with age in the young and adult cortex. However, the brain undergoes several dynamic changes throughout life, such as in the phases of early development and cognitive decline in the aging brain. We set out to search for intrinsic cellular changes in supragranular pyramidal cells across a broad age range: from birth to 85 years of age and we found differences in several biophysical properties between defined age groups. During the first year of life, subthreshold and suprathreshold electrophysiological properties changed in a way that shows that pyramidal cells become less excitable with maturation, but also become temporarily more precise. According to our findings, the morphological features of the three-dimensional reconstructions from different life stages showed consistent morphological properties and systematic dendritic spine analysis of an infantile and an old pyramidal cell showed clear significant differences in the distribution of spine shapes. Overall, the changes that occur during development and aging may have lasting effects on the properties of pyramidal cells in the cerebral cortex. Understanding these changes is important to unravel the complex mechanisms underlying brain development, cognition and age-related neurodegenerative diseases.

## Introduction

After birth, the brain undergoes developmental changes for a prolonged time that involve a series of complex and accurately orchestrated processes (Rakic 2009). The production and migration of neurons is largely complete at the beginning of postnatal development, and then the intrauterine developmental processes continue: gray and white matter thickening, myelination, synaptogenesis, pruning, and establishment of the basic anatomical architecture for initial neural pathway function. Subsequently, local connections within cortical circuits are fine-tuned, and increasingly complex, longer-term connections are established between circuits (Stiles 2010). After that, the changes do not end, but continue throughout human life. They are

mostly driven by environmental influences and experiences and lead to changes in metabolic activities (Kuzawa et al. 2014), changes in functional connectivity patterns (Kelly et al. 2009) and, with the maturation of white matter (Beck et al 2021, Yeatman et al 2014) changes in the speed of long-distance transmission (van Blooijs et al. 2023). The final phase is aging, where it slowly declines with advancing age, leading to a decline in cognitive signal processing functions and often resulting in neurodegenerative diseases (Peters 2006). The cortical supragranular glutamatergic cell (or pyramidal cell) provides the excitatory synaptic inputs for local inhibitory circuitry and other pyramidal cells by which they create distinct subnetworks (Yoshimura 2005). The development and formation of dendrites (Petanjek 2008, Koenderink 1995) and synapses (Huttenlocher and Dabholkar 1997) of pyramidal cells in the human cerebral cortex has been documented to some extent by postmortem studies, besides much less is known about their biophysical maturation and electrical properties in the early stages of development and the subsequent change or maintenance in later ages. Numerous studies demonstrated in non-primate animal models that the electrical characteristics of neurons change prominently in the early postnatal stage (Molnár et al. 2020). Changes in the intrinsic membrane properties (Picken Bahrey and Moody 2003), the input resistance or the kinetics of the elicited action potentials were reported (Kroon 2019, Elston and Fujita 2014) in connection with maturation of macaque and rodent pyramidal cells. To date, however, no cross-age studies have been conducted on the electrophysiological parameters of human pyramidal neurons. We have studied in detail the postnatal lifetime profile of the physiological and morphological properties of supragranular (layer 2/3) neurons of human pyramidal cells from neurosurgical resections. To this end, we performed whole-cell patch-clamp recordings and 3D anatomical reconstructions of human cortical pyramidal cells from 109 patients aged 1 month to 85 years for comprehensive data analysis to obtain the morphoelectric lifetime profile of supragranular pyramidal cells.

## Results

### Age-dependent differences in intrinsic subthreshold membrane properties

To extract biophysical properties of excitatory cells of human brain specimens we performed whole cell patch-clamp recordings of pyramidal cells from neurosurgically removed human neocortical tissue sections. The samples were mainly from the frontal and temporal lobes (Figure 1D, Supplementary Figure 1D), mostly from patients with tumors or hydrocephalus (Supplementary Figure 1B). Data were collected from 109 patients aged 1 month to 85 years (Figure 1B-C) from 498 human cortical layer 2/3 (L2/3) pyramidal cells. To confirm that the studied pyramidal cells originate from the L2/3, we measured the distance between the cell body and the L1 border (Berg 2021). 36% of the cells recovered their soma, with a distance of 129.69 ± 130.77 μm from the L1 border (Fig 1E). The data set was divided into seven age groups (Kang 2011, Bethlehem 2022): infant: < 1 year, early childhood: 1-6 years, late childhood: 7-12 years, adolescence: 13-19 years, young adulthood: 20-39 years, middle adulthood: 40-59 years, late adulthood: ≥ 60 years (Figure 1A).

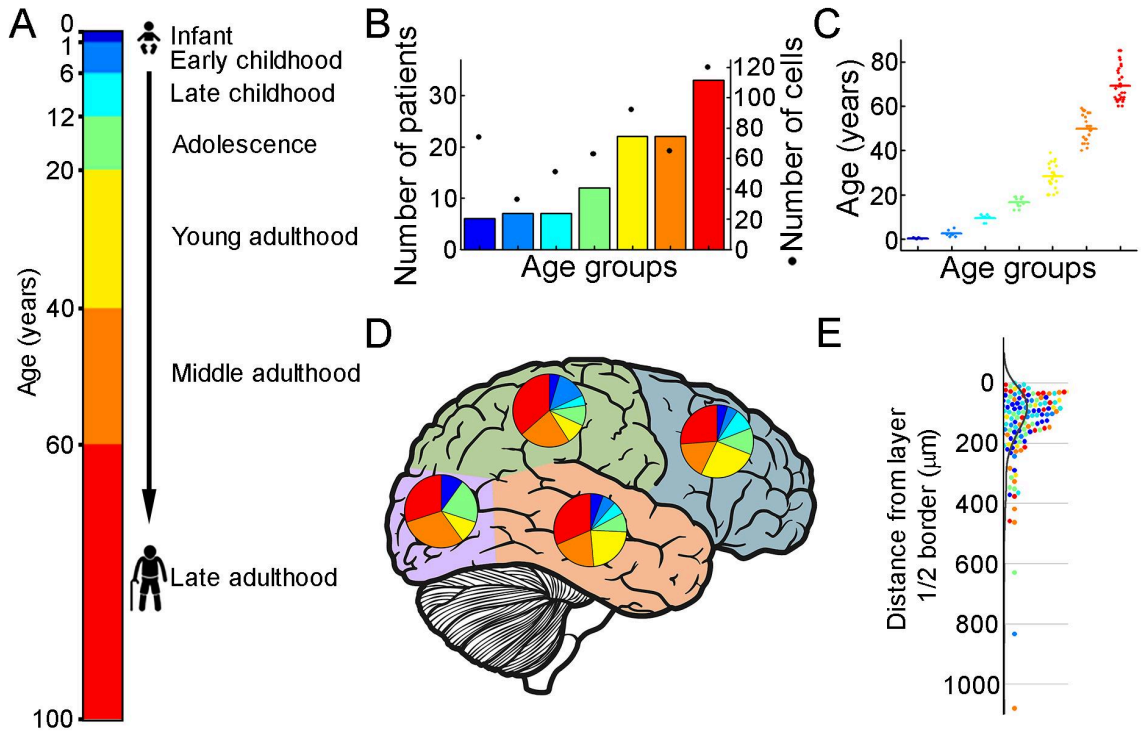


Figure 1. Illustration of the patient data on the samples utilized
(A) Illustration of the defined age groups.
(B) Number of patients involved in age groups, (n = 6, 7, 7, 12, 22, 22, 33 from infant to late adulthood, respectively). Dots show the number of human layer 2/3 pyramidal cells in our dataset regarding the defined age groups (n = 74, 33, 51, 63, 92, 66, 120 from infant to late adulthood, respectively).
(C) Distributions of patient ages within age groups.
(D) Brain model indicates the number of surgically removed tissues from the cortical lobes. Colors indicate age groups.
(E) The distribution of recovered cell bodies distance from the L1/2 border.

We evaluated the voltage deflections induced by negative and positive current injections and extracted subthreshold membrane features such as resting membrane potential, input resistance, time constant (tau), and sag ratio in 457 cortical pyramidal cells from 99 patients. We found that the subthreshold features from samples of infant significantly different from those from other age groups (Figure 2A-D; resting membrane potential: $P = 3.53\times10^{-8}$, input resistance: $P = 1.29\times10^{-16}$, tau: $P = 1.31\times10^{-15}$, sag ratio: $P = 5.2\times10^{-4}$, Kruskal-Wallis test) (Supplementary Figure 2). The resting membrane potential was significantly more positive in the first year of life than in the other age groups. Before adulthood a slight decrease was observed in the resting membrane potential across the groups (Table 1; Figure 2A). Input resistance, tau and sag ratio were measured on voltage deflections elicited by injecting negative (-100 pA) current steps into the cells. A significant decrease in input resistance (Table 1) was observed with the largest reduction after the first year of age ($P = 1.88\times10^{-6}$, Kruskal–Wallis test with post-hoc Dunn test) (Figure 2B). The membrane time constant also decreased significantly in

the older groups compared to the infant group, after infancy we found more conserved mean values of membrane time constant into older age (Table 1; Figure 2C). The ratio of the maximal deflection and the steady-state membrane potential during a negative current step (sag ratio) is significantly higher in late adulthood than in the early stages of life (Table 1; Figure 2D). Note that the high variance of the infant group data (e.g. resting membrane potential, input resistance, tau) are due to the dynamic change over the 0-1 year period (Supplementary Figure 3).

| **Subthreshold properties** | **Infant N = 72** | **Early childhood N = 28** | **Late childhood N = 45** | **Adolescence N = 54** | **Young adulthood N = 89** | **Middle adulthood N = 56** | **Late Adulthood N = 113** |
|---|---|---|---|---|---|---|---|
| | Mean ± SD | Mean ± SD | Mean ± SD | Mean ± SD | Mean ± SD | Mean ± SD | Mean ± SD |
| **Resting Vm (mV)** | -60.64 ± 9.86 | -65.44 ± 6.82 | -65.17 ± 6.68 | -67.86 ± 5.94 | -68.69 ± 5.54 | -65.14 ± 5.5 | -67.05 ± 7.86 |
| **Input resistance(MΩ)** | 257.25± 188.06 | 75.27 ± 37.5 | 74.61 ± 34.29 | 64.79 ± 41.82 | 70.45 ± 46.9 | 90.14 ± 54.37 | 81.14 ± 46.36 |
| **Tau (ms)** | 23.88 ± 14.7 | 8.49 ± 3.08 | 9.73 ± 4.24 | 8.99 ± 3.71 | 8.76 ± 6.33 | 8.53 ± 4.24 | 10.39 ± 6.63 |
| **Sag ratio** | 0.079 ± 0.87 | 0.075 ± 0.058 | 0.082 ± 0.092 | 0.086 ± 0.076 | 0.09 ± 0.084 | 0.092 ± 0.073 | 0.12 ± 0.1 |

Table 1. Subthreshold membrane properties
Table showing the mean and standard deviation of the passive parameters across the age groups.

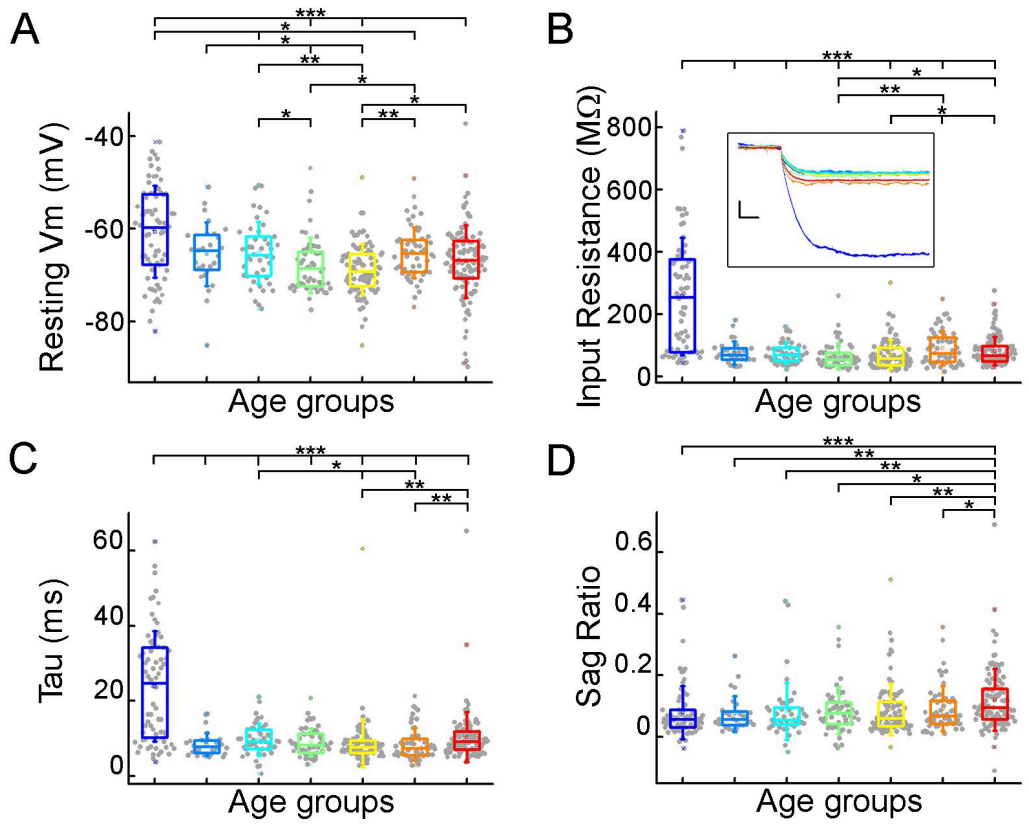


Figure 2. Subthreshold membrane properties vary across life stage

(A-D), Boxplots show resting membrane potential (A), input resistance (B), tau (C), and sag ratio (D) distributions in various age groups. (B) Inset shows representative voltage traces from each group. Scale bar: 5 mV; 20 ms. Asterisks indicate significance (Kruskal–Wallis test with post-hoc Dunn test, * $P < 0.05$, ** $P < 0.01$, *** $P < 0.001$).

**Suprathreshold properties across age-groups**

To initiate action potentials we injected positive current steps increased by 20 pA into the cells and recorded various types of input-output transformations. We extracted 25 features from different action potentials (AP) and firing patterns and assessed active membrane properties from recordings filtered for appropriate electrophysiological quality (see Methods). We found that the infant group differs most from the other age groups in several of the suprathreshold properties (Figure 3), but other trends are also apparent (rheobase current: $P = 8.71\times10^{-12}$, AP half-width: $P = 9.57\times10^{-25}$, AP up-stroke velocity: $P = 1.63\times10^{-12}$, AP amplitude: $P = 2.24\times10^{-11}$, Kruskal-Wallis test)(Supplementary Figure 4). For example, the average rheobase current, the minimum current that can trigger an action potential, is significantly lower in the early ages of life than in data collected from adolescence stage (Table 2) (infant vs. adolescence $P = 4.15\times10^{-13}$,Kruskal–Wallis test with post-hoc Dunn test). Further on the age scale we found that rheobase current was increased with age reaching a maximum value at the adolescent ages then declining to a significantly lower level (adolescent vs. late adulthood, $P = 5.23\times10^{-4}$, Kruskal–Wallis test with post-hoc Dunn test, Figure. 3A). The action potential (AP) half-width averages among a declining trend through the groups of age (Table 2) varied considerably across age groups forming significant differences between childhood and adulthood ages (Figure 3B). Action potential up-stroke velocities were significantly slower in the infant APs than in all the other ages (Table 2; Figure 3C). The amplitude of the elicited APs also showed age-dependent differences between age groups (Table 2); in the first year of life, the amplitude of APs were significantly lower than in other age groups. In adulthood, a significant decrease with age was observed (Figure 3D). Electrophysiological differences markedly separated the infant group from the older age groups shown on UMAP projection (Figure 3F, Supplementary Figure 5).

| **Suprathreshold properties** | **Infant N = 51** | **Early childhood N = 21** | **Late childhood N = 25** | **Adolescence N = 45** | **Young adulthood N = 63** | **Middle adulthood N = 43** | **Late Adulthood N = 83** |
|---|---|---|---|---|---|---|---|
| | Mean ± SD | Mean ± SD | Mean ± SD | Mean ± SD | Mean ± SD | Mean ± SD | Mean ± SD |
| **Rheobase (pA)** | 104.51± 103.18 | 218.1 ±123.27 | 252.8 ±131.17 | 306.22± 147.21 | 262.9 ± 148.06 | 219.07± 145.52 | 207.71± 107.83 |
| **AP half-width (ms)** | 1.68 ± 0.71 | 0.84 ± 0.15 | 0.88 ± 0.24 | 0.78 ± 0.22 | 0.76 ± 0.27 | 0.62 ± 0.17 | 0.74 ± 0.38 |
| **AP up-stroke (mV/ms)** | 247.43± 127.27 | 413.68 ±97.11 | 434.75 ±78.32 | 424.69 ± 87.58 | 418.49 ±110.33 | 419.15 ±129.29 | 379.22 ±118.45 |
| **AP amplitude (mV)** | 74.62 ± 13.4 | 90 ± 5.23 | 88.82 ± 6.35 | 86.31 ± 7.36 | 88.81 ± 8.52 | 87.28 ± 10.77 | 82.02 ± 8.49 |
| **F-I slope (Hz/pA)** | 0.142 ± 0.137 | 0.152 ±0.066 | 0.144 ± 0.071 | 0.139 ± 0.141 | 0.127 ± 0.08 | 0.176 ± 0.113 | 0.165 ± 0.117 |
| **First AP latency (ms)** | 161.26 ± 76.81 | 121.36 ± 76.88 | 115.29 ± 81.27 | 136.69 ±109.78 | 132.42 ± 84.68 | 140.61 ±143.43 | 106.39 ± 52.31 |
| **Adaptation** | 0.103 ± 0.087 | 0.061 ± 0.062 | 0.068 ± 0.06 | 0.105 ± 0.1 | 0.119 ± 0.118 | 0.114 ± 0.153 | 0.124 ± 0.1 |

Table 2. Action potential and firing pattern parameters

Table showing the mean and standard deviation of the suprathreshold properties across the age groups.

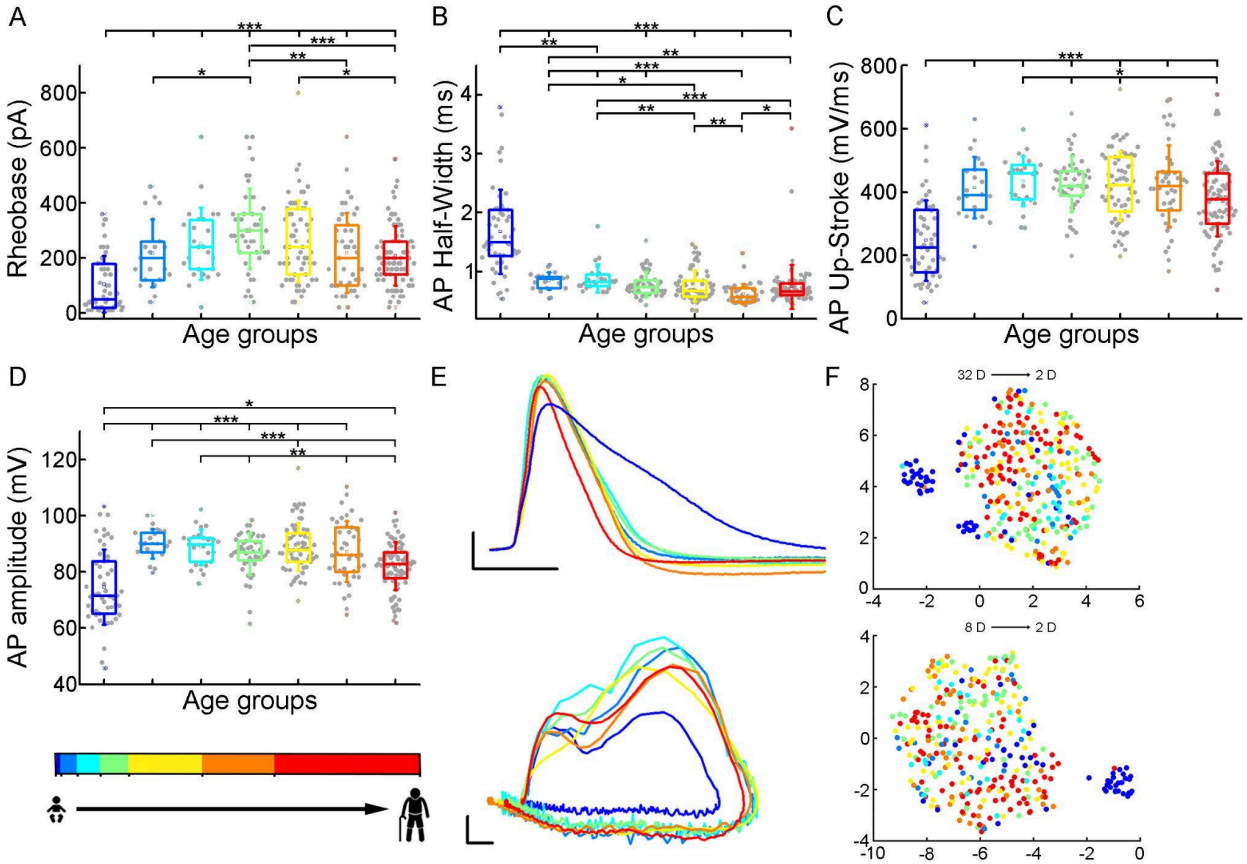


Figure 3. Age related differences in the action potential kinetics.

(A-D) Boxplots show differences in rheobase (A), action potential half-width (B), action potential up-stroke (C), and action potential amplitude (D) between the age groups. Asterisks indicate statistical significance (* P < 0.05, ** P < 0.01, *** P < 0.001).

(E) Representative action potentials aligned to threshold potential onset (scale: x axis: 1ms, y axis: 20 mV) (top) and phase plots of the representative APs (scale: x axis: 10 mV, y axis: 100 mV/ms) (bottom).

(F) Uniform Manifold Approximation and Projection (UMAP) of 32 (Table 4) (top) and 8 selected electrophysiological properties (resting Vm, input resistance, tau, sag ratio, rheobase, AP half-width, AP up-stroke and AP amplitude) (bottom) with data points for 331 cortical L2/3 pyramidal cells, colored with the corresponding age groups.

Next, we investigated how somatic current inputs are transformed to action potential output by evaluating the firing patterns of cells evoked by injecting prolonged positive current steps (Figure 4A) (Supplementary Figure 6). The neurons (n = 331) were regular spiking cells with moderate adaptation. The slope of the firing frequency versus the current curve (f-I slope) showed no significant difference across the age groups (P = 0.055, Kruskal-Wallis test) (Table 2; Figure 4B). Age related difference was observed in the latency of the first AP during rheobase

current injection (First AP latency), in the first year of life the latency of the first spike is significantly higher than all the other groups of age ($P = 7.67\times10^{-4}$, Kruskal-Wallis test), which is the most prominent with the oldest age group ($P = 8.41\times10^{-6}$, Kruskal–Wallis test with post-hoc Dunn test) (Table 2; Figure 4C). The adaptation of the AP frequency response to the same current injection stimulus also showed differences (P = 0.032, Kruskal-Wallis test) between the younger and the groups older than 13 years patients, we found the lowest adaptation values in early childhood (Table 2; Figure 4D).

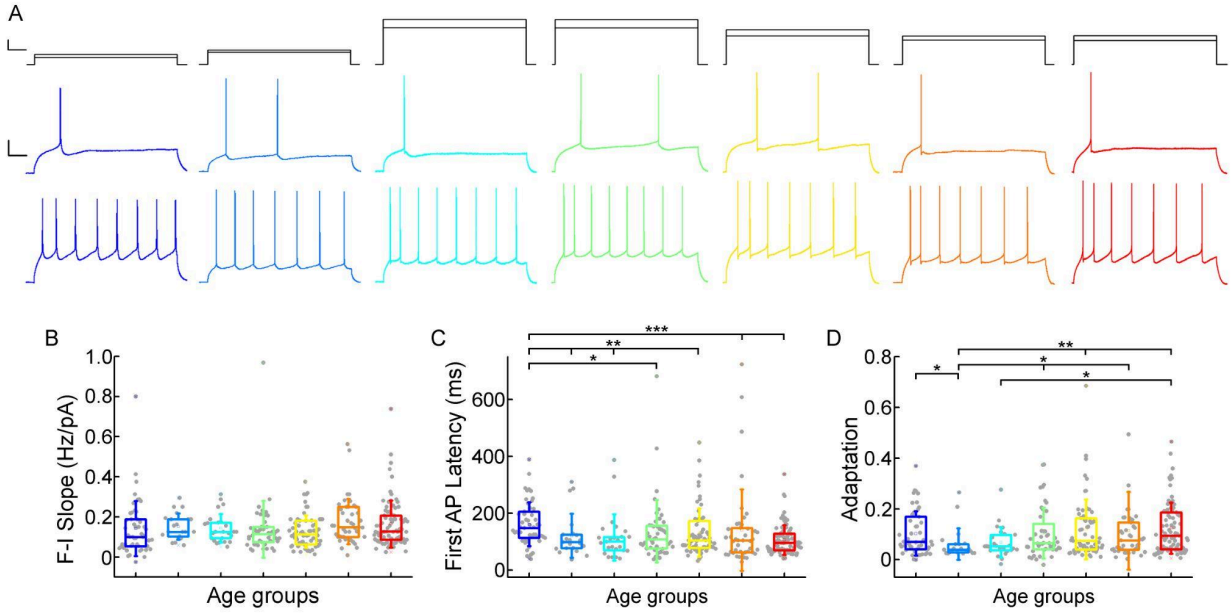


Figure 4. Age-dependency of the AP firing pattern parameters
(A) Representative membrane potential responses to an 800 ms long rheobase (middle) (left to right: infant, early childhood, late childhood, adolescence, young adulthood, middle adulthood, late adulthood), and increased current steps (bottom) Colored respectively to the age groups. Scale bar top: 1ms, 100 pA, bottom: 1ms, 20mV.
(B-D) Boxplots show changes across the age groups in f-I slope (B), first AP latency (C), and adaptation of APs (D). Asterisks indicate statistical significance (* P < 0.05, ** P < 0.01, *** P < 0.001).

Previous research has shown that the biophysical properties of the human pyramidal cells show depth-related correlations throughout the L2/3 (Berg 2021, Kalmbach 2018, Chameh 2021). Although there are some deeper cells in our dataset, the majority comes from the upper region of the L2/3. We compared the electrophysiological characteristics according to their depth from the border of L1 and L2 to exclude the possibility that the biophysical differences we found were a result of depth dependence. We did not find any overall differences related to distance of the soma from the L1 border within the age groups with a few exceptions. For example, the values of input resistance (P = 0.02, Mann-Whitney test) and AP up-stroke velocity (P = 0.04, Mann-Whitney test) differ significantly in the middle adulthood group. We found a significant

difference in AP amplitude (P = 0.02, Mann-Whitney test) and adaptation (P = 0.009, Mann-Whitney test) in the adolescence age group (Supplementary Figure 7-9).

**Morphological features of layer 2/3 pyramidal cells in different stages of life.**

To investigate possible morphological differences between the age groups, we filled the pyramidal cells with biocytin during recordings. Only neurons with no signs of deterioration and with complete apical dendrites and no signs of truncated dendritic branches or tufts were considered for morphological analysis. 63 pyramidal cells (Supplementary Figure 10) were reconstructed in 3D at ages 0-73 years (infant n = 7, early childhood n = 8, late childhood n = 11, adolescence n = 11, young adulthood n = 9, middle adulthood n = 9, late adulthood n = 8)(Supplementary Figures 11-12). Figure 5A shows examples of the reconstructed pyramidal cells. We did not detect significant change in total dendritic length (P = 0.37, Kruskal-Wallis test) (Table 3; Figure 5B), apical dendritic length (P = 0.6, Kruskal-Wallis test) (Table 3; Figure 5C), or basal dendritic length (P = 0.28, Kruskal-Wallis test) (Table 3; Figure 5D) at different ages. To investigate dendritic complexity we measured the total number of dendritic branching and found no significant developmental changes (P = 0.18, Kruskal-Wallis test) (Table 3; Figure 5E). We also did not observe significant differences in the size of dendritic branching when we measured the maximum horizontal (P = 0.64, Kruskal-Wallis test) (Table 3; Figure 5F) and vertical (P = 0.51, Kruskal-Wallis test) (Table 3; Figure 5G) extent of the reconstructed cells. We found significant differences in the average length of the uncut terminal segments of apical (P = 0.033, Kruskal-Wallis test) (Table 3; Figure 5H) but not of the basal dendrites (P = 0.85, Kruskal-Wallis test) (Table 3; Figure 5I) of the cells across the age groups.

| **Morphological properties** | **Infant N = 7** | **Early childhood N = 8** | **Late childhood N = 11** | **Adolescence N = 11** | **Young adulthood N = 9** | **Middle adulthood N = 9** | **Late adulthood N = 8** |
|---|---|---|---|---|---|---|---|
| | Mean ± SD | Mean ± SD | Mean ± SD | Mean ± SD | Mean ± SD | Mean ± SD | Mean ± SD |
| **Total dendritic length (mm)** | 6.74 ± 2.56 | 8.5 ± 4.56 | 6.62 ± 2.29 | 9.27 ± 4.82 | 6.76 ± 2.9 | 8.7 ± 2.7 | 8.96 ± 3.22 |
| **Apical dendritic length (mm)** | 3.77 ± 1.24 | 4.57 ± 2.42 | 3.78 ± 1.14 | 5.24 ± 2.51 | 3.88 ± 1.8 | 4.52 ± 1.63 | 4.64 ± 1.25 |
| **Basal dendritic length (mm)** | 2.97 ± 1.63 | 3.93 ± 2.74 | 2.84 ± 1.33 | 4.04 ± 2.44 | 2.88 ± 1.27 | 4.18 ± 1.35 | 4.31 ± 2.13 |
| **Total number of nodes** | 37.42 ± 23.58 | 40.88 ± 20.54 | 35.36 ± 12.07 | 48.36 ± 24.23 | 32.11 ± 12.38 | 47.33 ± 15.57 | 48.38 ±16.47 |
| **Max. horizontal extension (µm)** | 403.33±118.55 | 455.24 ±114.42 | 417.2 ±98.1 | 472.2 ± 104.51 | 448.3 ± 75.94 | 393.7 ± 90.29 | 420.93 ± 77.49 |
| **Max. vertical extension (µm)** | 498.12 ± 87.85 | 521.21 ± 102.88 | 463.83 ± 94.63 | 529.58 ± 129.28 | 447.41 ± 114.17 | 488.02 ± 81.02 | 490.45 ± 100.53 |
| **Apical terminal length (µm)** | 182.42 ± 48.17 | 204.83 ± 49.62 | 162.47 ± 21.5 | 189.59 ± 42.54 | 199.68 ± 36.2 | 151.23 ± 23.3 | 174.62 ± 36.76 |
| **Basal terminal length (µm)** | 142.54 ± 32.43 | 142.69 ± 30.31 | 138.7 ± 31.22 | 150.32 ± 26.09 | 155.29 ± 32.15 | 131.6 ± 30.44 | 148.96 ± 38.42 |

Table 3. Morphological properties
Table showing the mean and standard deviation of the morphological characteristics across the age groups.

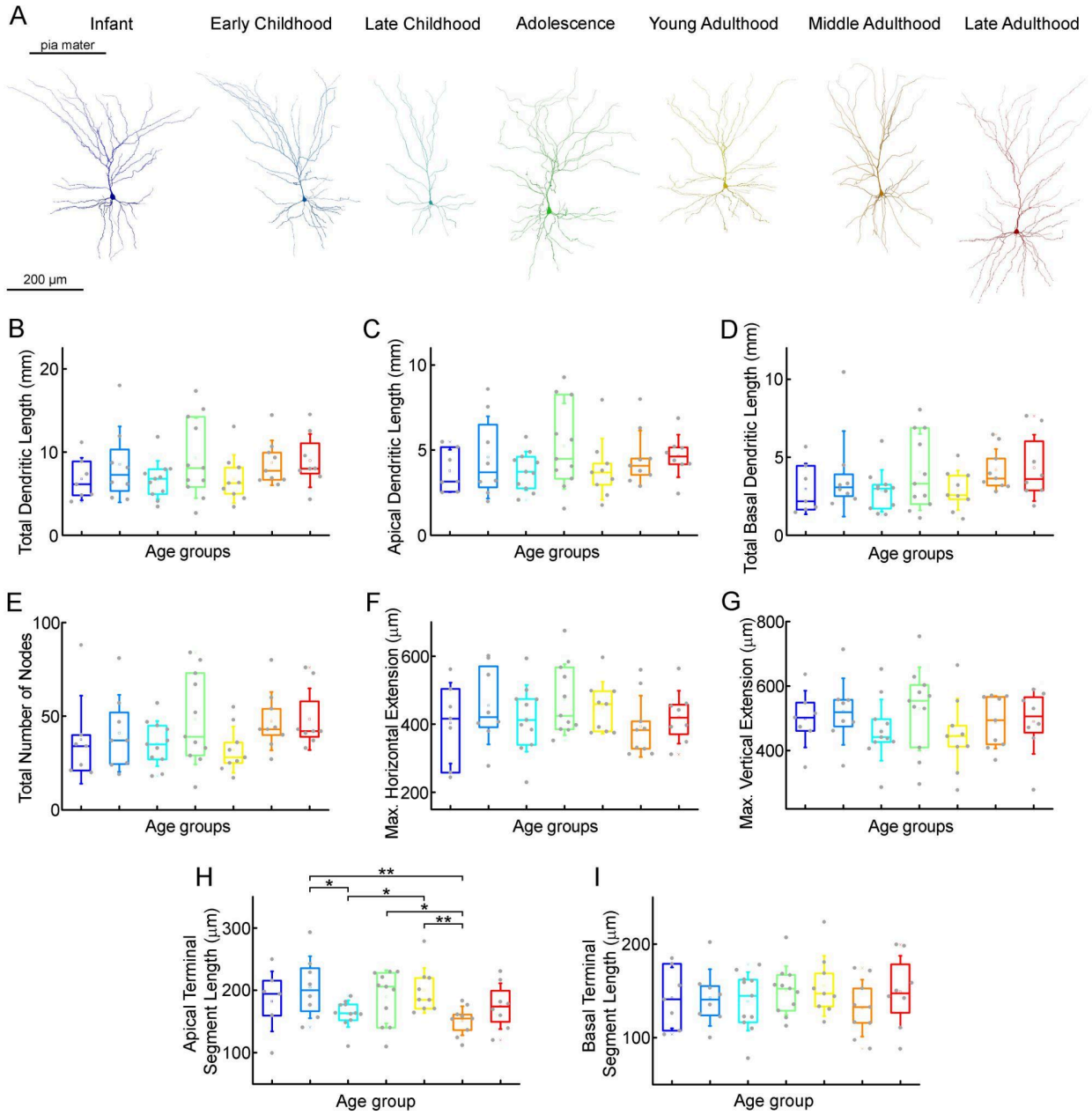


Figure 5. Morphological features of layer 2/3 pyramidal cells in different stages of life
(A) Representative reconstructions of L2/3 pyramidal cells (from left to right) from infant (n = 7), early childhood (n = 8), late childhood (n = 11), adolescence (n = 11), young adulthood (n = 9), middle adulthood (n = 9), and late adulthood (n = 8) patients.
(B-I) Boxplots show summarized data from all the reconstructed cells (Suppl. Fig. 7) of total dendritic length (B), apical dendritic length (C), total basal dendritic length (D), the total number of nodes on the apical and basal dendrites (E), the maximal horizontal (F), and the maximal vertical (G) extension of dendrites, the average length of the apical (H) and basal (I) terminal dendritic segments. Asterisks indicate statistical significance (* $P < 0.05$, ** $P < 0.01$, Kruskal-Wallis test with post-hoc Dunn test).

To analyze the distribution of dendritic spines we identified and labeled each spine on n = 6 fully 3D-reconstructed cells (Figure 6). We compared the spine density of selected pyramidal cells of two age groups: infant (83 days old, n = 3 of one patient, parietal lobe) vs. late adulthood (64.3 ± 2.08 years old, n = 3 of 3 patients, frontal, temporal and parietal lobes). The investigated cells are located in L2 (infant: 144.43 ± 45.26 μm, late adulthood: 161.22 ± 66.22 μm). We found that the total spine density was higher ($P = 7.57\times10^{-40}$, Mann-Whitney test) and also the spine density of both apical ($P = 2.02\times10^{-31}$, Mann-Whitney test) and basal ($P = 3.8\times10^{-12}$, Mann-Whitney test) dendrites was higher in the infant than in the late adult group (Figure 6B). To evaluate the age-dependence of spine morphology, we classified the spines into commonly used phenotypes based on their morphological characteristics (Li 2023), specifically distinguishing between mushroom-shaped, thin, filopodial, branched, and stubby spines (Figure 6C-G). Spines with large spine heads were classified as mushroom-shaped, those with small heads as thin, and long protrusions were distinguished as filopodial. Those that did not have peduncles were classified as stubby, spines with two heads emerging from the same spot were called branched spines (Figure 6C-G) (Luebke 2015). Only fully visible spines were included in the classification analysis. The composition of spine types varies between the two age groups, mushrooms are present at a higher percentage on apical branches in late adulthood cells ($P = 4.4\times10^{-9}$, Mann-Whitney test), and on the basal processes ($P = 9.04\times10^{-8}$, Mann-Whitney test) (Figure 6C,H). In contrast, thin spines and filopodia are present in significantly higher numbers on the apical (Figure 6D-E) (thin spines: $P = 7.34\times10^{-14}$; filopodia: $P = 1.11\times10^{-39}$, Mann-Whitney test) and basal (thin: $P = 2.46\times10^{-8}$; filopodia: $P = 2.14\times10^{-12}$, Mann-Whitney test) (Figure 6I-J) dendritic branches of the infant. Both apical and basal infant branches had a significantly higher percentage of branched spines (apical: $P = 1.64\times10^{-11}$; basal: $P = 8.9\times10^{-5}$, Mann-Whitney test) (Figure 6F,K), which were present in modest numbers on both. Stubby spines were also more prevalent on the elderly pyramidal cells, either on the apical ($P = 7.19\times10^{-5}$, Mann-Whitney test) or basal ($P = 6.97\times10^{-9}$, Mann-Whitney test) processes (Figure 6G,L). Comparing the spine density of the six individual cells, we found differences across the two age groups similar to those previously mentioned, alongside slight variation within age groups.(Supplementary Figure 13, Kruskal-Wallis test with post-hoc Dunn test).

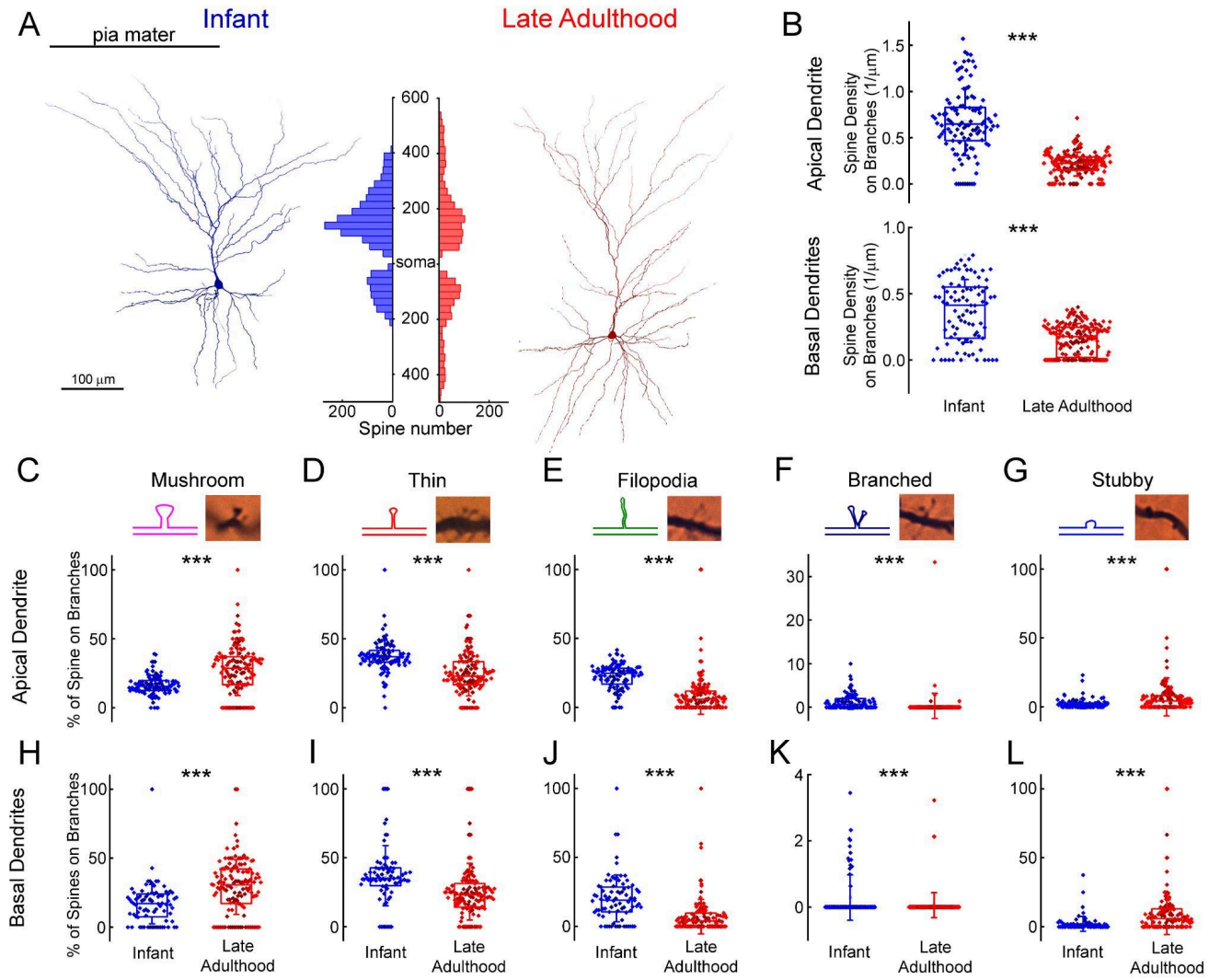


Figure 6. Comparison of dendritic spine densities in pyramidal cells from infant and late adulthood samples.

(A) Anatomical 3D reconstruction of human L2/3 pyramidal cells from the infant (left), and the late adulthood (right) age groups.The histogram (in the middle) demonstrates the distribution of dendritic spines on the two representative cells according to their distance from the soma (µm) on the apical and basal dendrites.

(B) Boxplots of the average spine densities on the apical (top), and basal (bottom) dendritic branches from the n = 3 infant (blue) and n = 3 late adulthood (red) L2/3 pyramidal cells. The symbols are color-coded by the 6 individual cells.

(C-G) The plots show the distribution of mushroom (C), thin (D), filopodium (E), branched (F), and stubby (G) dendritic spine types on the apical dendrites of the reconstructed infant (n = 3, blue) and late adult (n = 3, red) pyramidal cells. Top, schematic illustration and representative images of the examined dendritic spine types. Center, age dependent distribution of spine types. Asterisks indicate significance (* $P < 0.05$, ** $P < 0.01$, *** $P < 0.001$).

(H-L) Same as C-G but on basal dendrites.

Cortical tissue was dissected during neurosurgical procedures for various pathologies, but not to the same extent in the different groups. Specimen collection in adult/elderly patients was mostly for tumor resection, whereas in children hydrocephalus was the most common reason for brain surgery (Supplementary Figure 1). To determine the difference in medical condition could contribute to age-related differences in cellular features, we compared the extracted electrophysiological and morphological features based on the medical condition in the different age groups. It should be noted that all circumstances of surgical steps, tissue dissection, transport (time, media, temperature etc.) and cutting procedure remained the same in the different conditions. When comparing passive electrophysiological properties, we found no significant differences between the different medical conditions in the age groups from infancy to middle adulthood, only time constants were found to be significantly lower in the hydrocephalus patients than in the tumor patients in the young adulthood ($P = 0.048$, Mann-Whitney test) and late adulthood groups ($P = 0.01$, Mann-Whitney test) (Supplementary Figure 14). Comparing the action potential kinetics and firing pattern-related parameters between the different pathology groups we found no overall differences with some sporadic exceptions. For example, the parameters of AP half-width in young adulthood ($P = 0.01$, Mann-Whitney test) and the values of rheobase in early childhood ($P = 0.04$, Mann-Whitney test) differed significantly between the different pathologies (Supplementary Figure 15). Regarding the firing pattern-related properties we found significant changes in the infant F-I slope ($P = 0.02$, Mann-Whitney test), first AP latency ($P = 0.006$, two sample t-test) and adaptation ($P = 0.002$, Mann-Whitney test) parameters. Also in the late adulthood group the F-I slope ($P = 0.04$, Mann-Whitney test), the first AP latency ($P = 0.02$, Mann-Whitney test) and the adaptation ($P = 0.047$, Mann-Whitney test) were significantly different between the hydrocephalus and tumor patients (Supplementary Figure 16). Further comparison of morphological features revealed no statistical difference between tumor and hydrocephalus groups (Supplementary Figure 17).
To ascertain whether age-related variations in cell properties may be influenced by the gender of the patient, we compaired the examined characteristics of the cells by their sex (Supplementary Figure. 18-21). Comparing the passive membrane properties of the cells in different age groups we found higher resting membrane potential values in adolescent females than in males ($P = 0.04$, Two-sample t-test) and input resistance was lower in female patients in the late childhood group ($P = 0.03$, Mann-Whitney test) (Supplementary Figure 18). We found differences when comparing the AP characteristics in AP half-with cells from male patient showed higher values in early childhood ($P = 0.036$) and adolescence ($P = 0.02$). AP up-stoke velocity was higer in young adulthood females than in males ($P = 0.34$). AP amplitude was significantly higher in male patients in early childhood ($P = 0.003$) and late adulthood ($P = 0.035$) age groups (Supplementary Figure 19). Under the comparison of the firing pattern features cells from the infancy showed significant differences in F-I slope ($P = 0.2$, Mann-Whitney test), first AP latency ($P = 0.0096$, Two-sample t-test) and adaptation ($P = 0.002$, Mann-whitney test). The latency of the first AP was higher in cells from male patient in the young ($P = 0.03$, Mann-Whitney test) and middle ($P = 0.018$, Mann-Whitney test) adulthood cells. The adaptation of the APs in males was higher during adolescence ($P = 0.027$, Mann-Whitney test) but lower in middle adulthood ($P = 0.034$, Mann-Whitney test)(Supplementary Figure 20). Regarding the morphological property of the reconstructed cell we found differences in the young adulthood age group between cells from male and female

patients in total (P = 0.03, Mann-Whitney test) and apical (P = 0.03, Mann-Whitney test) dendritic length and the total number of bifurcations (P = 0.03, Mann-Whitney test), in the middle adulthood group we found significant difference in the average apical terminal length across males females(P = 0.03, Mann-Whitney test)(Supplementary Figure 21).

## Discussion

In this study, using the whole-cell patch-clamp technique and 3D reconstructions, we have studied the differences of human cortical L2/3 pyramidal cells at various stages of life. We found that during the lifespan the most significant changes take place early in life during the first year in most of the biophysiological characteristics of human pyramidal cells (see Supplementary Figure 3). We recorded from n = 457 human cortical excitatory pyramidal cells from the supragranular layer from birth to 85 years. Most differences in sub- and suprathreshold features were found in the youngest age groups. There were particular differences in resting membrane potential, input resistance, time constant, rheobasic current, AP halfwidth and AP upstroke velocity. Other age groups that differed the most from other age groups were the oldest (60 - 85 years) with modest differences in sag ratios. In our morphological analysis, we found no significant changes in the overall apical and basal dendritic dimensions across different ages. When evaluating the number of spines in two anatomical reconstructions (from the infant and late adulthood groups) we found a higher overall spine density in the infant than in the elder sample consisting of mainly branched and thin spines and filopodia. In contrast, stubby and mushroom-shaped spines were more prevalent in the older pyramidal cell.

The nervous system experiences a multitude of plastic changes throughout an individual's lifetime. These changes extend from the early stages of development and continue through the gradual degenerative processes that come with old age. Although precise intrinsic cellular modifications linked to aging remain somewhat elusive, there is an observable morphological transformation during early development. As the nervous system matures, dendritic branching (Kasper et al. 1994, McAllister 2000) and cell body size increases (Zhang 2004). Also, learning and experience increase the extent of dendritic branching (Holloway 1966, Greenough and Volkmar 1973) and dendritic spines (Globus 1973). An extensive body of research has shown that synaptic plasticity induces formation of new dendritic spines and the enlargement of existing spines (Kastellakis 2023). These modifications may affect the input-output relation of a neuron as model studies suggest that dendritic geometry influences electrical and firing properties (Mainen and Sejnowski 1996, van Elburg and van Ooyen 2010, Eyal 2014, Vetter et al 2001). Furthermore, in parallel to the changes in morphological complexity there is ample experimental evidence that the maturation of ion channels and the change in increasing channel density in the neuronal membrane also play a role in influencing the electrical properties of neurons (Huguenard et al. 1988, Connors 1994). These findings point to a close causal relationship between structure and electrophysiological properties at cellular level.

*Lifespan changes in electrophysiological properties*

The intrinsic electrophysiological properties of a neuron are determined by several factors: the resistivity of the cytoplasm and membrane, the membrane capacitance, and the shape of the soma and dendrites. The basic passive parameters we recorded, such as the resting membrane potential, the input resistance, and the membrane time constant show a dramatical change in the first year. This change is consistent with data found in previous studies on neocortical pyramidal cells from rodent models (Kasper 1994, Kroon 2019, Picken Bahrey and Moody 2003, Zhang 2004, Zhu 2000, McCormick 1987) and on xenotransplated human cortical neurons (Linaro 2019). We found a progressive shift of the resting membrane potential from -60 mV to -68 mV in the first part of the lifespan (<40 years), which could be due to the age-dependent change in ion channel composition (Picken Bahrey and Moody 2003). The input resistance and time constant showed a sudden and sharp decrease between the first and second age groups, indicating the most dramatic changes in the infant brain followed by a generalized and slower decrease. As pyramidal cells mature, the size and volume of the cell body increase (Petanjek 2019, Zhu 2000) which correlates with the input resistance, meaning that a small membrane area has a higher input resistance (Luhmann 2000). In addition to the increase in cell surface area, the increase in the expression of certain potassium leak channels, e.g. from the two-pore domain potassium channel (KCNK) family, can also influence the input resistance during cell maturation (Aller 2008, Goldstein 2001). Similar reasons can lead to a decrease in the membrane time constant. The membrane time constant is the product of the specific input resistance and the specific membrane capacitance. Assuming constant membrane capacitance (~1 $pF/cm^2$, Oláh et al 2024, Beaulieu-Laroche 2018), the decrease is likely also due to a change in specific membrane resistance. The result of developmental changes in membrane passive parameters during early development improves spike timing precision and temporal responsiveness in the cortical microcircuit (Oswald and Reyes 2011, Doischer et al. 2008). However, in our human samples at later ages (>40 years) that we associate with the aging brain, the previous trends of changes in intrinsic characteristics are reversed. Input resistance and time constant increase, which may be associated with the decline in KCNK expression in the aging brain (Erraji-Benchenkroun 2005). These membrane parameters are also generally higher in studies in rhesus monkeys (Moore 2023), except for the resting membrane potential, which is not different from that of young cortical L2/3 (Chang 2005) or L5 pyramidal cells (Luebke 2007) in the brain. However, in our samples, we found a positive shift in the resting potential between the middle- and old-age groups by a few millivolts. It should be noted that this discrepancy may be due to the fact that the age groups in our work are not the same as the works mentioned.

Changes in resting membrane potential and input resistance will add up to produce a rising and then falling curve of the averaged rheobasic current, with the value three times higher in the adolescent group than in the youngest group and 1.5 times higher than in late adulthood. Our results on increased rheobase during early life are consistent with previous studies in rodent cortical L3 and 5 pyramidal cells (Kroon 2019, Perez-García 2021, Popescu 2021) and with findings regarding aging in rhesus monkey cortical neurons from rhesus monkeys (Moore 2023).

When we assessed the voltage sag ratio with age we found a consistent increase that peaked in late adulthood. The voltage sag that occurs during membrane hyperpolarization is the result of activation of the hyperpolarization-activated cyclic nucleotide-gated (HCN) current, also known as the h-current. Similar to our findings the age-dependent increase in sag deflection has

been observed in human cortical pyramidal cells (Guet-McCreight 2023, Kalmbach 2018) which is consistent with studies by Wang et al. (2011, 2007) that have linked inhibited HCN activation to working memory deficits in the elderly.

The electrical output of neurons is driven by the composition of neuronal molecules and ion channels whose expressions and distributions change most dynamically in two periods, early development, and the aging brain. This dynamic essentially produced an inverted U-shaped curve in the distribution of the active electrical properties over the lifespan in our dataset, an increase in the first year, a relatively stable middle phase, and then a return in older age groups. The origin of these changes is mainly due to changes in the distribution of sodium and potassium channels. During development, there is evidence that the number of voltage-gated $Na^+$ channels increases in rodents (Huguenard et al. 1988, Picken Bahrey and Moody 2003) and in humans (Erraji-Benchekroun 2005), which may accelerate the kinetics of the action potential (up-stroke) and, similar to our results, increase the amplitude of the action potential (Perez-García 2021, Kroon 2019, Zhang 2004, McCormick 1987, Etherington 2011). During aging, however, regulation is disrupted by the change in channel expression, which can lead to altered conduction rate of ionic currents. In brain senescence, the amplitude of the action potential and a slowing of the action potential (Luebke 2007) have been shown to be similar to our data, which may be caused by the decreased expression of voltage-gated $Na^+$ channels (Erraji- Benchekroun 2005).

We examined the firing patterns of pyramidal cells at different ages by comparing the F-I slope, and we found that the patterns are fairly conserved across ages. In rodent developmental studies, a decrease in F-I slope was found only in the first two weeks after birth (Zhang 2004, McCormick 1987), which time window is not represented in our data. The latency of the first spike is influenced by the time-constant and specific ion channels, like the transient (or A-type) $K^+$ current and the transient $Ca^{2+}$ current (or T-type) (Molineux 2005). The same ion channels are involved in burst firing at the onset of stimulation. Note that in our sample only ~10 % of pyramidal cells showed burst firing at the beginning of stimulation, but it is known that burst firing is more frequent from layer 3 onwards at depth (Berg 2021). The presence of A-current has been found in immature pyramidal neurons from sensorimotor areas in rodent studies (McCormick 1987), and the density of T-type currents also remains unchanged during the development of the visual cortex (Horibe 2014). It has been shown that the expression of the T-type calcium channel family (CACNG3) decreases during aging (Erraji-Benchekroun 2005). However, it must be mentioned that the differences in the expression of all subtypes of the Kv4 (A-type) and $Ca_V3.x$ (T-type) channel families during brain development and aging have not been systematically described.

*Properties of dendritic trees and spine distribution with age*

Transcriptomic analyses of the human neocortex show relatively stable expression patterns of genes for dendritic and synaptic development after about 1 year of age (Kang 2011). In early postmortem studies human pyramidal neurons were studied for morphological changes as a function of age. In these studies, using Golgi staining methods, it was found that the dendritic trees of infant layer 2/3 pyramidal cells are well developed (Mrzljak et al. 1990). In the human prefrontal cortex after birth, the dendritic tree of layer 3 pyramidal neurons reaches its

structurally mature form after about 3 months (Petanjek 2008). Thereafter, it is assumed that a smaller increase in dendritic length reaches its final form between about 7.5-12-months (Koenderink 1995, Petanjek 2008). In our study, we observed stable patterns of apical and basal dendrite lengths and dendritic tree complexity across the lifespan. Even between the early postnatal groups (infancy vs. early childhood), no significant difference in dendritic tree size was observed. This can be explained by the influence of various factors, such as the large difference between individual subjects or the subtype specific dendritic morphology of pyramidal cells (Berg et al 2021) or different maturation curves of neurons from different brain regions (Elston and Fujita 2014) or cortical layers (Petanjek 2008).

Neurons exhibit a phase of synaptogenesis overproducing synapses lasting months or years in the human cortex (Huttenlocher 1979, Huttenlocher et al. 1982, Mrzljak et al. 1990, Petanjek et al. 2011), followed by dendritic spine/synapse pruning that is reported to last more than a decade in the cortex (Petanjek et al. 2011, Jacobs 1997, Mavroudis 2015, Benavides-Piccione 2013, Coskren 2015). Our results from comparing two groups: infant and late adult pyramidal cells also show that the overall number of dendritic spines decreases with increasing age. When evaluating the distribution of spine shapes in young and old pyramidal cells, we found spines with larger heads (mushroom shape) in a greater number in the dendrite of old pyramidal cells, which are considered as mature synapses. The size of the head is an indicator of the size of the postsynaptic density, the number of glutamate receptors, and the strength of the synapse (Bourne and Harris 2008, Matsuzaki 2001, Nusser 1998). In the developing nervous system, however, the filopodia, thin dendritic protrusions without a head, are the most characteristic type of spines. The density of filopodial spines was higher on the dendrites of infant pyramidal cells. In the older cells, we still found filopodia, which are the silent precursor of active synapses (Vardalaki 2022). The change in the ratio of subtypes from young to old age is well established and is associated with the basis for changes in cognitive function during aging (Luebke 2015, Dumitriu 2010, Jacobs 1997).

The complexity of human brain activity and cognitive abilities increases with development and decreases with aging, resulting in an inverted U-shaped curve across the lifespan (Craik and Bialystok 2006). Cognitive functions depends on many age dependent factors, such as the density and specificity of synaptic connections formed by synaptic pruning and plasticity, or the degree of myelination and white matter maturation and there is also an age-related modulation of neurotransmitters, hormones, ion transporters and receptors (Luna 2015). Here we have shown that pyramidal cells become less excitable and temporarily more precise during development by changing their intrinsic functional properties and with aging these changes occur somewhat in opposite directions making the intrinsic parameters change symmetrically. In addition some of the changes are asymmetrical either occur with development or with aging, such as the resting membrane potential which mostly changes in young ages or the ratio of sag, which is shifted most in old age. These changes in the intrinsic properties of cells during the first and last stages of life also contribute to the input-output functions of a neuron and ultimately to the age-related development of cognitive abilities.

## Materials and methods

### Slice preparation

Experiments were performed according to the Declaration of Helsinki with the approval of the University of Szeged Ethical Committee and Regional Human Investigation Review Board (ref. 75/2014). Prior to surgery, the patients provided written consent for all tissue material. We used human cortical tissue adjacent to the pathological lesion that had to be surgically removed from patients (n = 64 female n = 45 male) as part of the treatment for tumors, hydrocephalus, apoplexy, cysts, and arteriovenous malformation. Anesthesia was induced with intravenous midazolam and fentanyl (0.03 mg/kg, 1–2 µg/kg, respectively). A bolus dose of propofol (1–2 mg/kg) was administered intravenously. The patients received 0.5 mg/kg rocuronium to facilitate endotracheal intubation. The trachea was intubated, and the patient was ventilated with a mixture of $O_2$-$N_2O$ at a ratio of 1:2. Anesthesia was maintained with sevoflurane at a care volume of 1.2–1.5. During the surgical procedure tissue blocks were removed from parietal (n = 22), temporal (n = 35), frontal (n = 42), and occipital (n = 10) regions, the resected tissue blocks were immediately immersed in ice-cold solution. Slices were cut perpendicular to the pia mater at a thickness of 320 µm with a vibrating blade microtome (Microm HM 650 V) in ice-cold solution (in mM) 75 sucrose, 84 NaCl, 2.5 KCl, 1 $NaH_2PO_4$, 25 $NaHCO_3$, 0.5 $CaCl_2$, 4 $MgSO_4$, 25 D(+)-glucose, saturated with 95% $O_2$ and 5% $CO_2$. The slices were incubated in the same solution for 30 minutes at 36°C following that the solution was changed to (in mM) 130 NaCl, 3.5 KCl, 1 $NaH_2PO_4$, 24 $NaHCO_3$, 1 $CaCl_2$, 3 $MgSO_4$, 10 D(+)-glucose, saturated with 95% $O_2$ and 5% $CO_2$, the slices were kept in it until use.

In vitro electrophysiological recordings

Somatic whole-cell current-clamp recordings were obtained at ~36 °C in solution containing (in mM) 130 NaCl, 3.5 KCl, 1 $NaH_2PO_4$, 24 $NaHCO_3$, 3 $CaCl_2$, 1.5 $MgSO_4$, 10 D(+)-glucose, from layer 2/3 pyramidal cells visualized by infrared differential interference contrast (DIC) video microscopy equipped with micromanipulators (Luigs and Neumann, 652 Ratingen, Germany) and HEKA EPC 9&10 patch clamp amplifier (HEKA Elektronik GmbH, Lambrecht, Germany). Micropipettes (3-5 MΩ) were filled with intracellular solution containing (in mM) 126 potassium-gluconate, 4 KCl, 4 ATP-Mg, 0.3 GTP-$Na_2$, 10 HEPES, 10 phosphocreatine, and 8 biocytin (pH 7.20; 300 mOsm). After whole-cell configuration was obtained stepwise currents were injected to measure the evoked sub- and suprathreshold membrane potential properties. For the analysis of the electrophysiological recordings n = 457 recordings with a series resistance (Rs) of 24.93 ± 11.18 MΩ (max: 63.77 MΩ) were used. For the analysis of fast parameters related to the action potential (AP half-width, AP upstroke velocity, AP amplitude and rheobase), higher quality requirements were set and cells with Rs > 30 MΩ were excluded. This reduced the data set to n = 331 cells with Rs 19.42 ± 6.2 MΩ.

Data analysis

Electrophysiological features were measured from voltage responses elicited by 800 ms long current steps increasing by 20 pA from -100 pA. We analyzed the electrophysiological data with Fitmaster software (HEKA Elektronik GmbH, Lambrecht), and custom MATLAB (The Math Works, Inc.) scripts.

Analysis of morphological features was made by NeuroExplorer software (MBF Bioscience, Williston, VT, USA) and Origin 9 (OriginLab, Northampton, MA).

| | |
|---|---|
| Resting Vm | The membrane potential of the neuron, measured directly after attaining the whole-cell configuration with no current (if a holding current was used during the recording we compensated the resting membrane potential with the injected current). |
| Input resistance | To calculate input resistance the mean of all hyperpolarizing current produced voltage steps were used. |
| Tau | To calculate time constant the mean of all hyperpolarizing current produced voltage steps were used, measured between 0-63%. |
| Sag ratio | The ratio of the maximal deflection and the steady-state membrane potential during a -100 pA current step. |
| Rheobase | The minimal current step that elicited the first spike. |
| AP half-width | The width of the AP at half amplitude. |
| AP up-stroke | The mean of all the maximum values of dV/dt between the action potential onset and the action potential peak from each elicited APs of the cell. |
| AP amplitude | Average amplitude of all APs, from threshold to peak. |
| F-I slope | The slope of the line fitted to the data of the AP firing frequency versus stimulus intensity. |
| First AP latency | The duration from the start of the stimulus until the first AP under the rheobasic current step. |
| Adaptation | The average adaptation of the interspike interval between consecutive APs. |
| Rebound | The difference between the steady-state membrane potential and the maximum deflection after a hyperpolarizing current step. |
| Rebound-Sag ratio | The ratio of the rebound and sag amplitudes. |
| Avg. AP number | Average number of elicited APs per sweep. |
| AP threshold | Mean of all the voltage values at AP threshold. |
| Ap rise time | Mean time between the threshold and the peak of all APs. |
| AHP amplitude | Average amplitude of all afterhyperpolarization. |
| AHP length | Average duration of 0 (AHP minimum) to 90% of all the AHP. |
| Voltage at max.dV/dt | Average voltage value at the maximum of the AP dv/dt over all APs |
| Velocity at min. dV/dt | Average velocity value at the minimum of the AP dv/dt from all APs |
| Voltage at min. dV/dt | Average voltage value at the minimum of the AP dv/dt from all APs |
| AP peak | Average of AP maximum voltages |
| ISI mean | Average interspike interval from all sweeps containing at least three APs |
| AP amplitude accommodation | The difference of the first and last AP amplitude in a sweep. |
| AP half-width accommodation | The difference of the first and last AP half-width in a sweep. |
| AP threshold accommodation | The difference of the first and last AP threshold in a sweep. |
| Average ISI | The mean value of interspike intervals in a sweep. |
| AP amplitude adaptation | The average adaptation of the AP amplitude between consecutive APs. |
| AP half-width adaptation | The average adaptation of the AP half-width between consecutive APs. |
| AP threshold adaptation | The average adaptation of the AP threshold between consecutive APs. |
| AHP area | Integral of the AHP from the minimum value to 90%, using trapezoidal method. |
| ADP amplitude | The amplitude of the afterdepolarization, the average difference between the minimum value of the AHP and the threshold of the next AP. |

Table 4. Examined electrophysiological properties

Statistics

We used custom-written R scripts (R 4.1.2) and the gamm function from the mgcv R package (mgcv 1.8.38). Data presented as the mean ± s.d. Normality was tested with the Lilliefors test, for statistical analysis, ANOVA with posthoc Bonferroni test, Kurskal-Wallis with posthoc Dunn test, for pairwise comparison two-sample t-test or Mann-Whitney test was used. Differences

were accepted as significant if $p < 0.05$. The data are shown on boxplots, boxes indicate 25th, 50th (median), and 75th percentiles, rectangle represents the mean value, and whiskers indicate s.d.

Histology and reconstruction

Slices were fixed in a fixative of 4% paraformaldehyde, 15% picric acid, and 1.25% glutaraldehyde in 0.1 M phosphate (PB, pH = 7.4) for at least 12 hours after electrophysiological recording. After multiple washes in 0.1 M PB, slices were cryoprotected in 10% then 20% sucrose solution in 0.1 M PB. The slices were frozen in liquid nitrogen and then thawed in PB. Slices were embedded in 10% gelatin and further sectioned into 70 μm thick sections. Sections were incubated in a solution containing conjugated avidin-biotin horseradish peroxidase (ABC; 1:100; Vector Labs) in Tris-buffered saline (TBS, pH = 7.4) overnight at 4°C. The enzyme reaction became visible by using 0.05% 3'3-diaminobenzidine tetrahydrochloride as a chromogen and 0.01% $H_2O_2$ as an oxidant. Sections were post-fixed with 1% $OsO_4$ in 0.1 M PB. Following several washes with distilled water, sections were stained in 1% uranyl acetate, and dehydrated in an ascending series of ethanol. The sections were infiltrated with epoxy resin (Durcupan, Sigma-Aldrich) overnight and embedded on glass slides. After the electrophysiologically recorded cells have been visualized by DAB staining, 3D light microscopic reconstructions were carried out using the Neurolucida system (MBF Bioscience, Williston, VT, USA) with a 100× objective. The length of terminal segments was measured between the terminal tip of the dendrites and the last branching point before the terminal tip. Dendritic spine density on the dendritic branches was calculated as spine/μm between two bifurcations. The percentage of spines on branches was calculated as the percentage of the given spine type from all the types of spines on that branch.

**Acknowledgements**

The authors thank Éva Tóth, Katalin Kocsis, Leona Mezei, Otília Kelemen and Bettina Lehóczki for assistance in anatomical experiments and Gergely Komlósi, Szabina Horváth-Furdan, Ildikó Piszár, Sándor Lovas, Balázs Kovács, Rajmund Lákovics, Márton Rózsa, Gáspár Oláh, Attila Ozsvár, Joanna Grace Sandle and Zoltán Péterfi for electrophysiological recordings.

**Funding**

This work was supported by Eötvös Loránd Research Network grants HUN-REN-SZTE Agykérgi Neuronhálózatok Kutatócsoport and KÖ-36/2021 (G.T.)
Ministry of Human Capacities Hungary (20391-3/2018/FEKUSTRAT and NKP 16-3-VIII-3)(G.T.); National Research, Development and Innovation Office grants GINOP 2.3.2-15-2016-00018, Élvonal KKP 133807, ÚNKP-20-5 - SZTE-681, 2019-2.1.7-ERA-NET-2022-00038, TKP2021-EGA-09, TKP-2021-EGA-28 (G.T.) ÚNKP-21-5-SZTE-580
National Institutes of Health awards U01MH114812 (G.T.) and UM1MH130981 (G.T.)

## Supplementary figures and tables

| Age (years) | Sex | Brain region | Hemisphere | Surgical procedure |
|---|---|---|---|---|
| 0.66 | female | T | right | tumor removal |
| 0.08 | male | T | right | shunt |
| 0.28 | male | O | left | shunt |
| 0.1 | female | F | left | tumor removal |
| 0.23 | male | P | right | shunt |
| 0.67 | male | F | left | shunt |
| 2 | male | F | left | shunt |
| 1 | female | F | right | shunt |
| 4 | male | T | left | tumor removal |
| 5 | female | P | right | tumor removal |
| 2 | male | P | right | shunt |
| 2 | female | P | right | shunt |
| 1 | female | TO | left | shunt |
| 7 | male | F | right | tumor removal |
| 7 | male | P | right | tumor removal |
| 10 | male | F | left | tumor removal |
| 10 | female | F | left | tumor removal |
| 11 | female | F | right | tumor removal |
| 11 | male | T | left | shunt |
| 10 | male | T | right | other |
| 13 | female | F | right | tumor removal |
| 16 | male | PO | right | tumor removal |
| 18 | male | F | right | tumor removal |
| 18 | female | T | left | tumor removal |
| 19 | male | O | right | shunt |
| 19 | female | F | right | tumor removal |
| 19 | male | P | right | shunt |
| 16 | male | T | right | tumor removal |
| 13 | female | T | right | other |
| 15 | female | F | right | shunt |
| 15 | female | O | left | shunt |
| 19 | female | F | right | tumor removal |
| 28 | female | F | right | tumor removal |
| 27 | female | F | right | other |
| 20 | male | T | right | tumor removal |
| 30 | female | F | right | shunt |
| 25 | female | O | right | shunt |
| 29 | female | T | left | other |
| 25 | female | FT | left | tumor removal |
| 23 | female | T | right | other |
| 26 | female | F | right | shunt |
| 30 | male | F | left | tumor removal |
| 21 | female | F | right | shunt |
| 35 | male | T | right | tumor removal |
| 35 | female | TO | left | tumor removal |
| 39 | female | F | left | tumor removal |
| 36 | male | T | left | tumor removal |
| 32 | male | T | right | tumor removal |
| 33 | male | F | right | shunt |
| 34 | male | P | left | tumor removal |
| 20 | male | F | right | shunt |
| 30 | female | F | right | tumor removal |

| Age (years) | Sex | Brain region | Hemisphere | Surgical procedure |
|---|---|---|---|---|
| 45 | female | F | right | tumor removal |
| 41 | male | T | right | shunt |
| 53 | male | T | right | tumor removal |
| 55 | female | T | left | tumor removal |
| 43 | male | T | right | tumor removal |
| 51 | female | F | right | other |
| 46 | female | P | right | shunt |
| 58 | male | T | left | tumor removal |
| 57 | female | T | right | tumor removal |
| 58 | female | T | left | tumor removal |
| 47 | female | F | right | tumor removal |
| 51 | male | O | left | shunt |
| 43 | male | F | right | shunt |
| 59 | female | P | right | shunt |
| 57 | female | O | right | shunt |
| 43 | female | O | right | shunt |
| 56 | female | F | left | shunt |
| 51 | male | FT | left | tumor removal |
| 49 | female | F | right | tumor removal |
| 40 | female | P | right | tumor removal |
| 49 | male | O | right | tumor removal |
| 70 | male | T | left | tumor removal |
| 72 | female | T | right | tumor removal |
| 81 | female | O | right | shunt |
| 63 | male | F | right | tumor removal |
| 65 | male | T | right | tumor removal |
| 69 | female | P | left | other |
| 70 | female | P | right | shunt |
| 77 | male | P | right | shunt |
| 79 | female | P | right | shunt |
| 63 | female | T | right | tumor removal |
| 64 | male | T | left | tumor removal |
| 69 | female | O | right | shunt |
| 66 | female | F | right | tumor removal |
| 75 | female | O | left | shunt |
| 78 | female | T | right | shunt |
| 60 | female | T | right | tumor removal |
| 60 | female | F | right | tumor removal |
| 62 | female | F | right | shunt |
| 62 | female | T | right | tumor removal |
| 62 | female | P | left | tumor removal |
| 63 | female | F | right | tumor removal |
| 63 | female | O | right | tumor removal |
| 63 | female | F | left | tumor removal |
| 63 | female | F | right | shunt |
| 64 | male | F | right | tumor removal |
| 76 | male | F | right | tumor removal |
| 85 | male | FT | right | shunt |
| 85 | female | O | left | shunt |
| 82 | female | T | right | other |
| 73 | male | T | right | tumor removal |
| 68 | female | T | right | tumor removal |

| | | | | |
|---|---|---|---|---|
| 26 | female | P | left | tumor removal |
| 20 | male | T | right | tumor removal |
| 45 | male | P | right | shunt |
| 66 | female | P | right | shunt |
| 64 | male | FP | left | tumor removal |

Supplementary table 1. Patient metadata
Table showing the patients age, gender, brain region (F - frontal, T - temporal, P - parietal, O - occipital, PO - parieto-occipital, FT - fronto-temporal, TO - temporo-occipital, FP - fronto-parietal), hemisphere and the surgical procedure.

| | **Infant** | | | | | **Late adulthood** | | | | |
|---|---|---|---|---|---|---|---|---|---|---|
| | **#1 cell** | **#2 cell** | **#3 cell** | **Mean** | **SD** | **#1 cell** | **#2 cell** | **#3 cell** | **Mean** | **SD** |
| **Total spine number** | 3039 | 5883 | 4443 | 4455 | 1422.04 | 1909 | 2977 | 1553 | 2146.33 | 741.07 |
| **Apical spine number** | 2352 | 3256 | 3568 | 3058.67 | 631.56 | 1237 | 1282 | 849 | 1122.67 | 238.07 |
| **Basal spine number** | 687 | 2627 | 875 | 1396.33 | 1069.93 | 672 | 1695 | 704 | 1023.67 | 581.61 |
| **Mushroom** | 477 | 970 | 762 | 736.33 | 247.5 | 629 | 1085 | 407 | 707 | 345.66 |
| **Thin** | 1055 | 2157 | 1666 | 1626 | 552.09 | 455 | 680 | 403 | 512.67 | 147.23 |
| **Filopodia** | 732 | 1431 | 936 | 1033 | 359.45 | 223 | 154 | 105 | 160.67 | 59.28 |
| **Branched** | 31 | 62 | 53 | 48.67 | 15.95 | 5 | 1 | 2 | 2.67 | 2.08 |
| **Stubby** | 67 | 99 | 84 | 83.33 | 16.01 | 83 | 247 | 134 | 154.67 | 83.93 |
| **Not classified** | 677 | 1164 | 942 | 927.67 | 243.82 | 514 | 810 | 502 | 608.67 | 174.46 |

Supplementary table 2. Number of dendritic spines on the examined cells.
Table showing the overall number of dendritic spines, the total number of spines on the apical and basal dendritic arbour and the number of dendritic spines from different phenotypic subtypes of the individual pyramidal cells (n = 3 infant and n = 3 late adulthood).

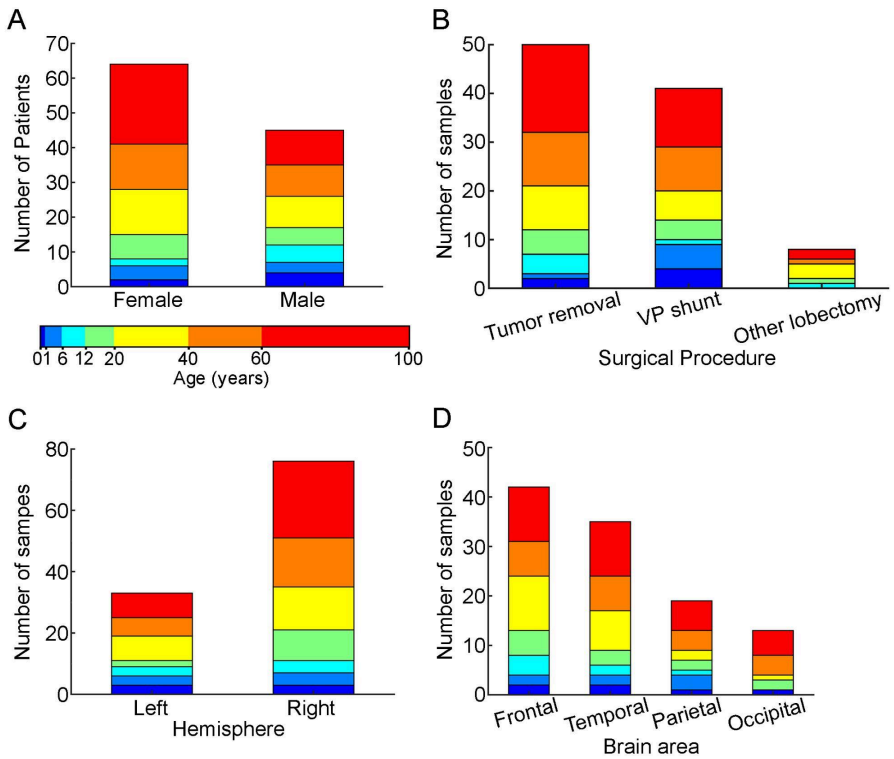


Supplementary Figure 1. Patient metadata
Distribution of patients by gender (female: infant n = 2, early childhood n = 4, late childhood n = 2, adolescence n = 7, young adulthood n = 13, middle adulthood n = 13, late adulthood n = 23, male: infant n= 4, early childhood n = 3, late childhood n = 5, adolescence n = 5, young adulthood n = 9, middle adulthood n = 9, late adulthood n = 10) (A), surgical procedure (tumor removal: infant n = 2, early childhood n = 2, late childhood n = 5, adolescence n = 7, young adulthood n = 13, middle adulthood n = 12, late adulthood n = 19, VP (ventriculoperitoneal) shunt: infant n= 4, early childhood n = 5, late childhood n = 1, adolescence n = 4, young adulthood n = 6, middle adulthood n = 9, late adulthood n = 12, other: infant n= 0, early childhood n = 0, late childhood n = 1, adolescence n = 1, young adulthood n = 3, middle adulthood n = 1, late adulthood n = 2) (B), hemisphere (left: infant n = 3, early childhood n = 3, late childhood n = 3, adolescence n = 2, young adulthood n = 8, middle adulthood n = 6, late adulthood n = 8, right: infant n= 3, early childhood n = 4, late childhood n = 4, adolescence n = 10, young adulthood n = 14, middle adulthood n = 16, late adulthood n = 25) (C) and brain area (frontal: infant n = 2, early childhood n = 2, late childhood n = 4, adolescence n = 5, young adulthood n = 11, middle adulthood n = 7, late adulthood n = 11, temporal: infant n = 2, early childhood n = 2, late childhood n = 2, adolescence n = 3, young adulthood n = 8, middle adulthood n = 7, late adulthood n = 11, parietal: infant n = 1, early childhood n = 3, late childhood n = 1, adolescence n = 2, young adulthood n = 2, middle adulthood n = 4, late adulthood n = 6, occipital: infant n = 1, early childhood n = 0, late childhood n = 0, adolescence n = 2, young adulthood n = 1, middle adulthood n = 4, late adulthood n = 5)(D). Stacked columns are colored regarding the age groups shown on the colorbar.

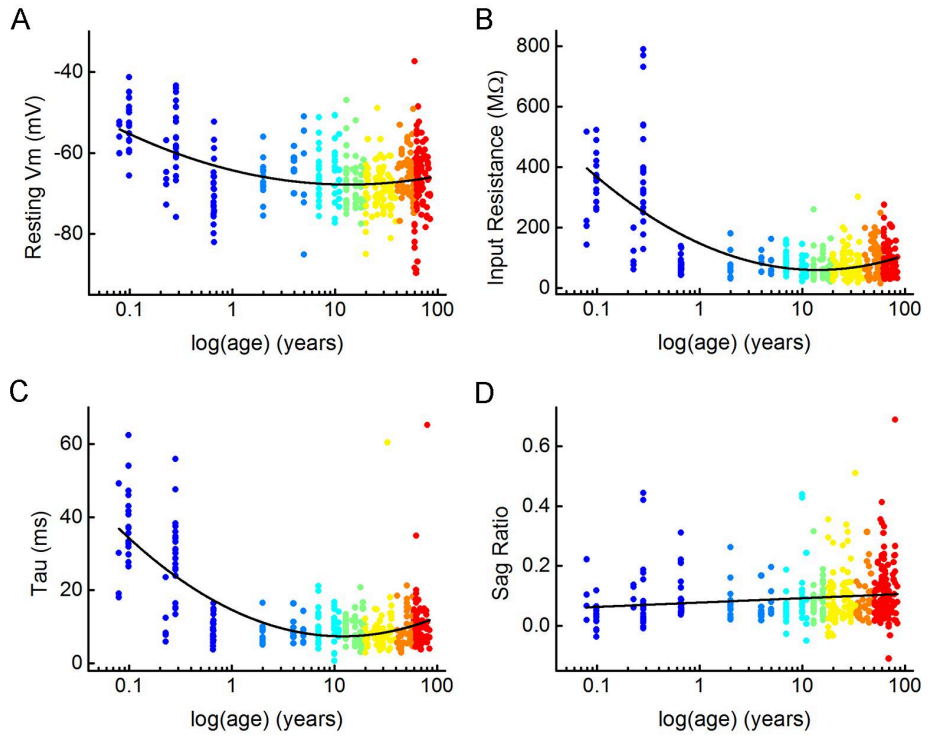


Supplementary Figure 2. Distribution of subthreshold electrophysiological features with age. (A-D) Scatter plots showing the passive electrophysiological characteristics: resting membrane potential (A), input resistance (B), tau (C), and sag ratio (D) throughout the lifespan. Dots are colored according to the age groups, age is represented in years on a logarithmic scale.

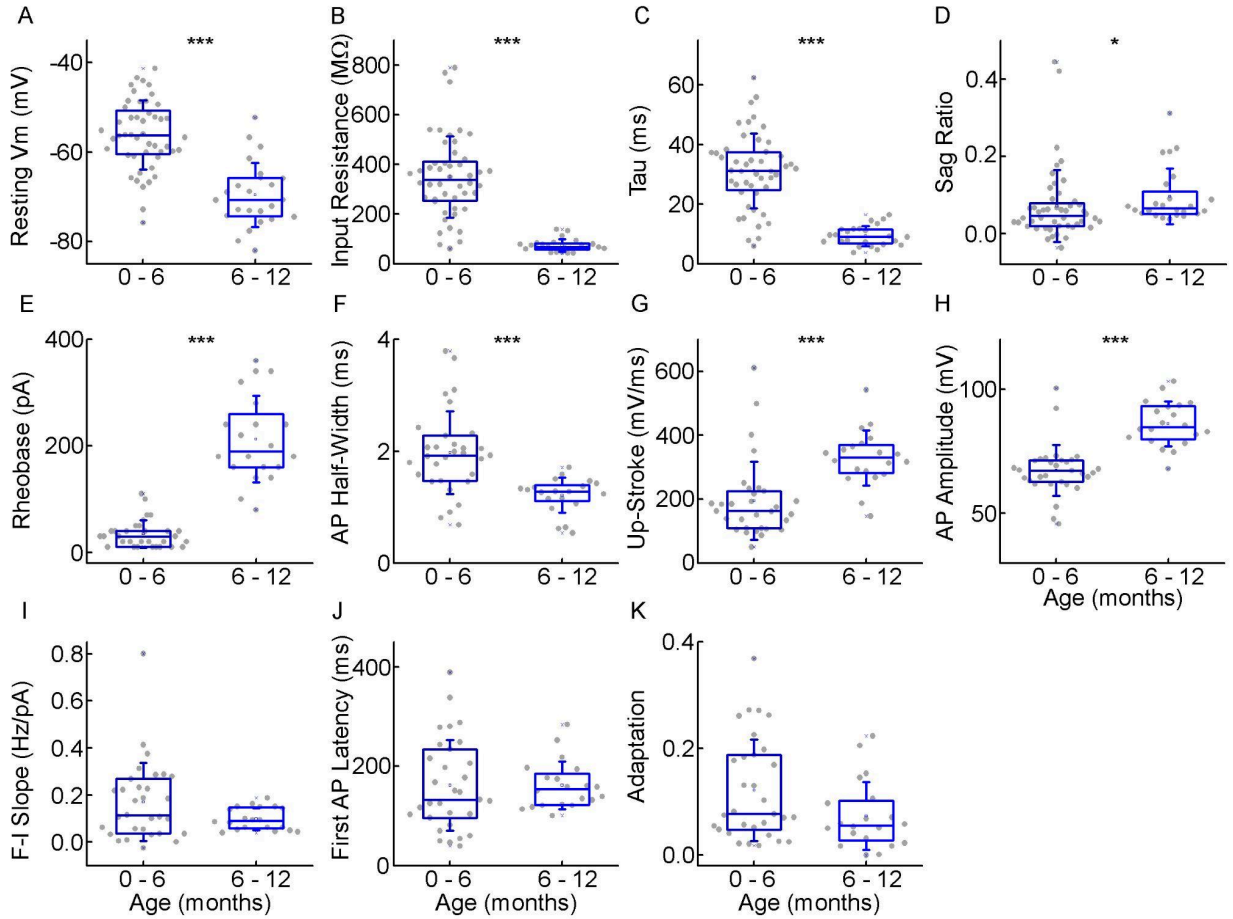


Supplementary Figure 3. Electrophysiological differences during the first year of life

A-D, Boxplots showing differences in passive properties, resting membrane potential (A), input resistance (B), tau (C) and sag ratio (D) within the infant age group (* P < 0.05, ** P < 0.01, *** P < 0.001, two sample t-test (A, B, C) or Mann-Whitney test (D)).

E-H, Differences in the action potential kinetics, Rheobase (E), AP half-width (F), up-stroke (G), and AP amplitude (H) between the cells from the first and the second half of the first year of life. Asterisks indicate significance (* P < 0.05, ** P < 0.01, *** P < 0.001, Mann-Whitney test).

I-K, Deviations in AP firing pattern parameters, F-I slope (H), first AP latency (I), and adaptation (J) during infancy.

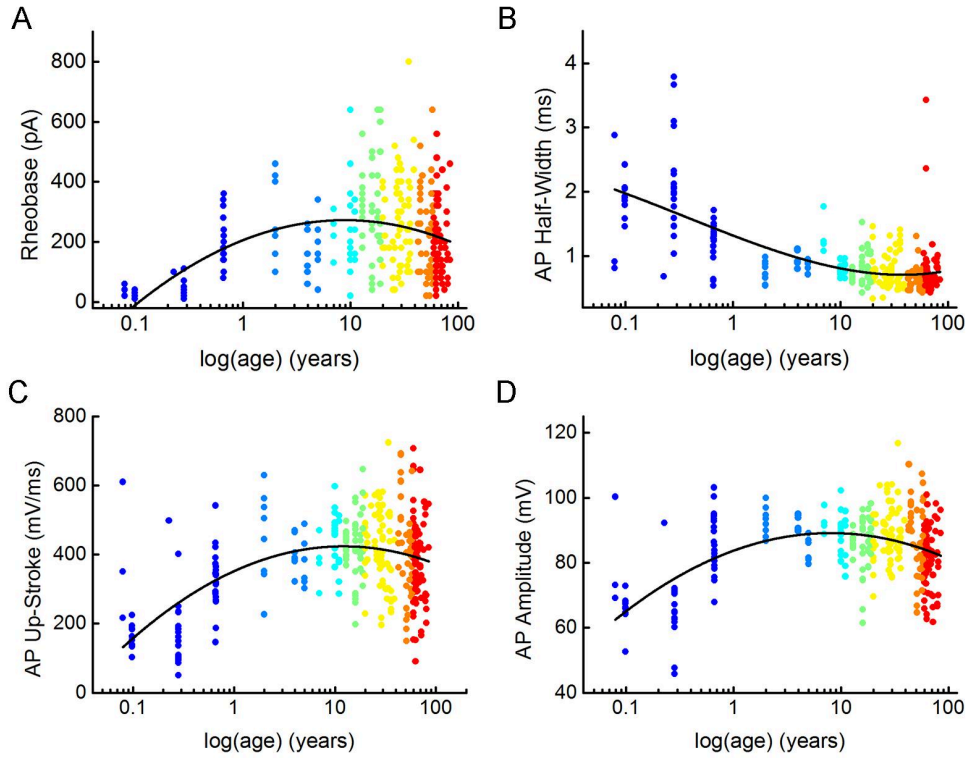


Supplementary figure 4. Distribution of suprathreshold electrophysiological features with age. (A-D) Diagrams show changes through age in rheobase (A), action potential half-width (B), action potential up-stroke (C), and action potential amplitude (D). Dots are colored according to the age groups, age is represented in years on a logarithmic scale.

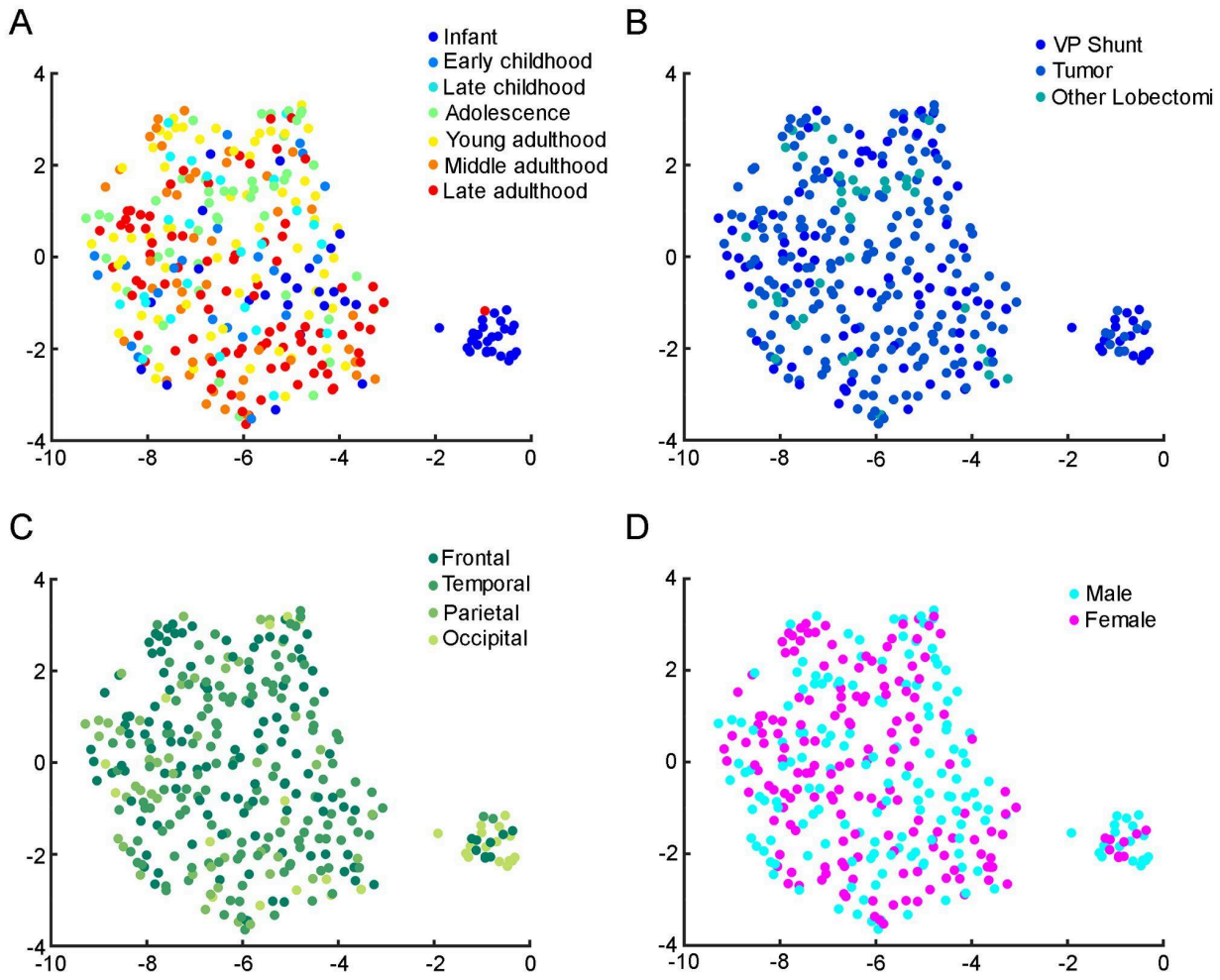


Supplementary Figure 5. Relationship between patient metadata and electrophysiology. Uniform Manifold Approximation and Projection (UMAP) of 8 electrophysiological properties (resting Vm, input resistance, tau, sag ratio, rheobase, AP half-width, AP up-stroke, and AP amplitude) with data points for 331 cortical L2/3 pyramidal cells, colored with the corresponding age groups (A), surgical procedures (B), brain area (C) and gender (D).

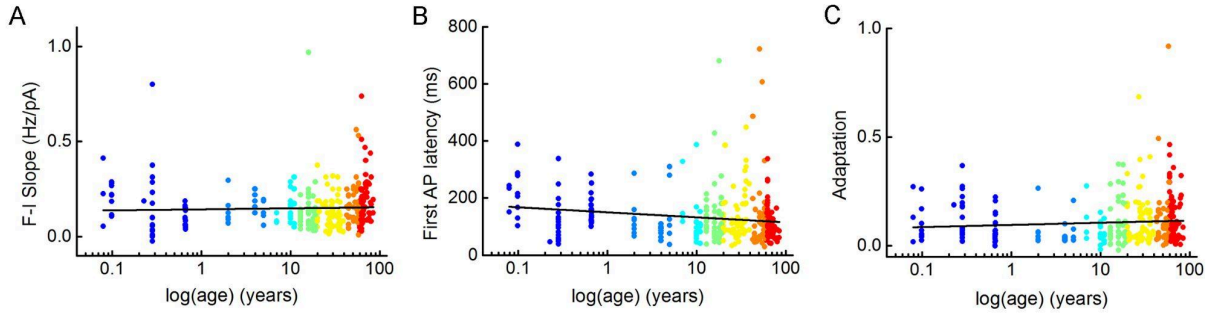


Supplementary Figure 6. Distribution of firing pattern characteristics with age.

(A-C) Plots show F-I slope (A), first AP latency (B), and adaptation of APs (C) depending on age. Dots are colored according to the age groups, age is represented in years on a logarithmic scale.

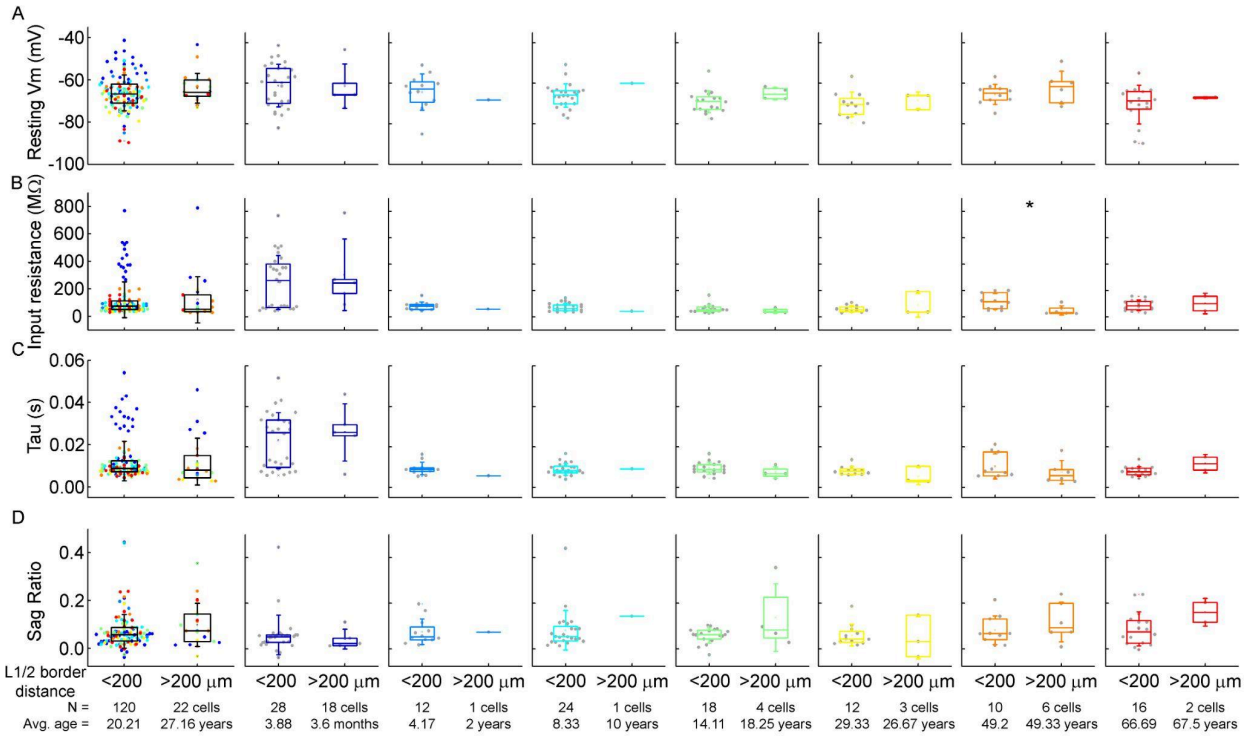


Supplementary Figure 7. Comparison of the subthreshold properties of the cells as a function of their distance from the layer border.
A-D: Box plots show resting membrane potential (A), input resistance (B), tau (C), and sag ratio (D) of the pyramidal cells whose soma is located at a distance greater than and less than 200 µm from the L1 border. From left to right: data from all age groups, infant, early childhood, late childhood, adolescence, young adulthood, middle adulthood and late adulthood groups. Asterisks indicate significance (* $P < 0.05$, Mann-Whitney test).

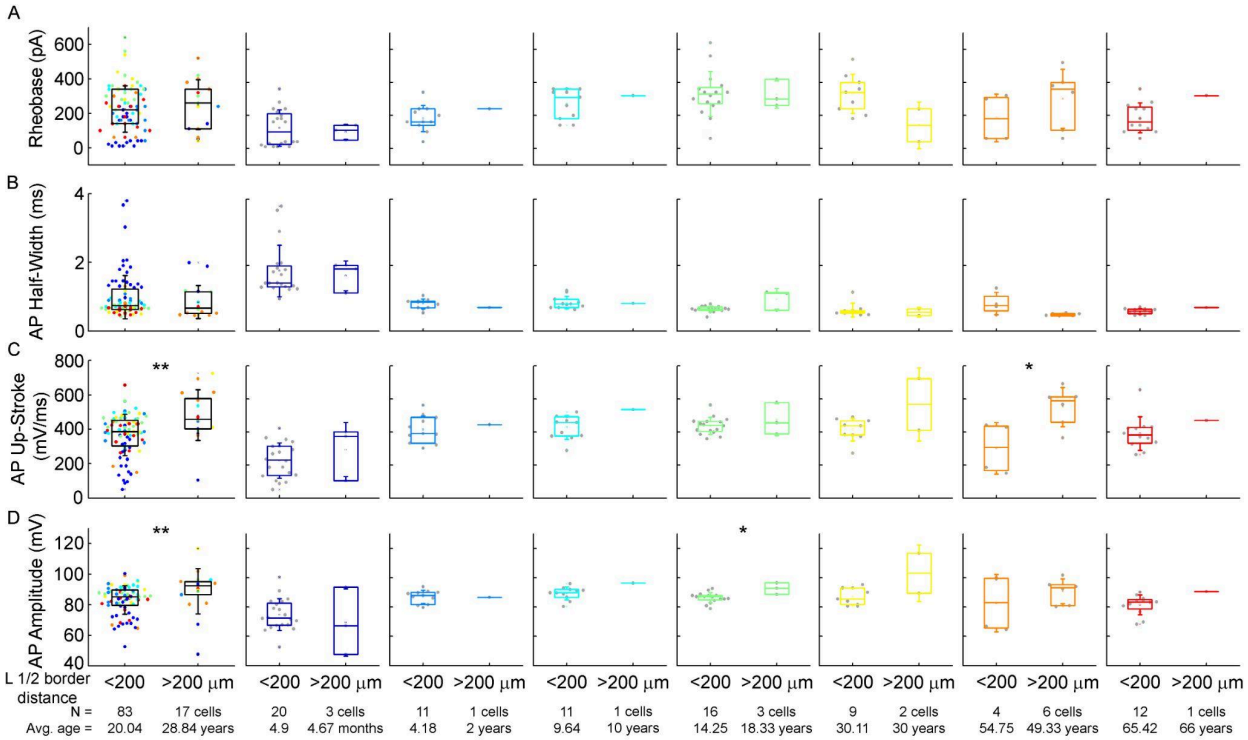


Supplementary Figure 8. Comparison of the action potential properties of the cells as a function of their distance from the layer border.

A-C: Boxplots show rheobase (A), action potential half-width (B), action potential upstroke (C) and action potential amplitude (D) of cells whose soma is located at a distance greater than and less than 200 µm from the L1 border. From left to right: data from all age groups, infant, early childhood, late childhood, adolescence, young adulthood, middle adulthood and late adulthood. Asterisks indicate significance (* P < 0.05, ** P < 0.01, Mann-Whitney test).

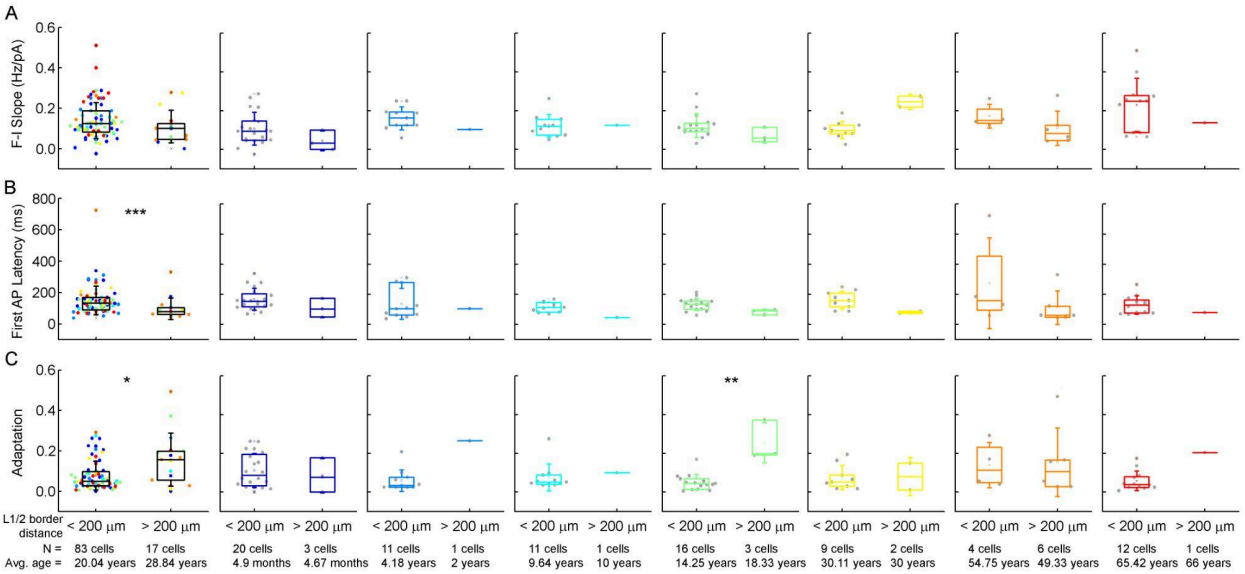

Supplementary Figure 9. Comparison of the firing pattern characteristics of the cells as a function of their distance from the layer border.
A-C: Boxplots show: F-I slope (A), latency of the first AP (B) and adaptation of APs (C) of cells whose soma is located at a distance greater than and less than 200 μm from the L1 border. From left to right: data from all ages, infancy, early childhood, late childhood, adolescence, young adulthood, middle adulthood and late adulthood. Asterisks indicate significance (* $P < 0.05$, ** $P < 0.01$, Mann-Whitney test).

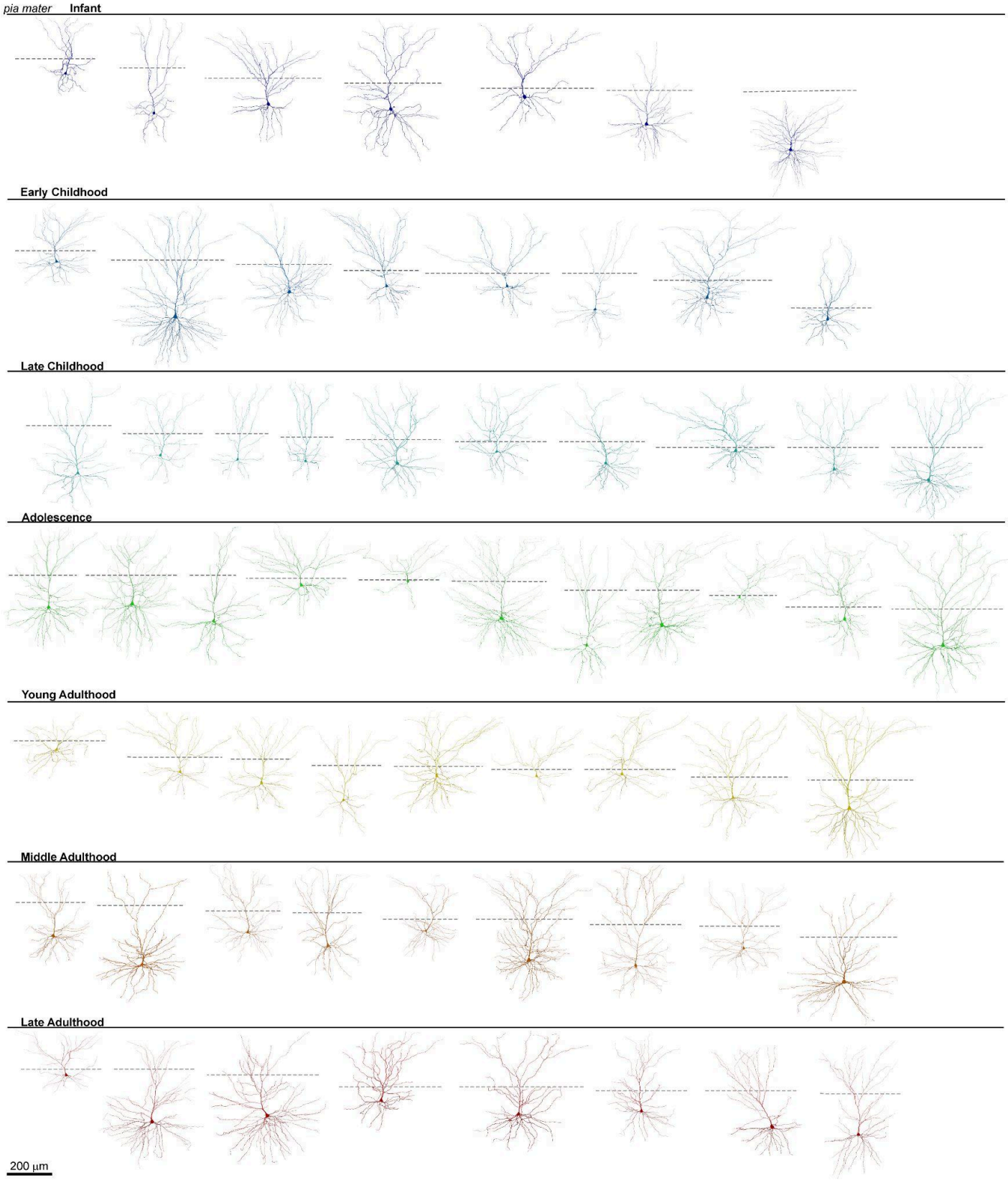


Supplementary Figure 10. Human cortical L2/3 pyramidal cell dendritic reconstructions.

Reconstructions (n = 63) of the examined human cortical pyramidal cells, from top to bottom: infant, early childhood, late childhood, adolescence, young adulthood, middle adulthood and late adulthood age groups. Black lines are representing the pia mater, gray dashed lines represent the L1-L2 border.

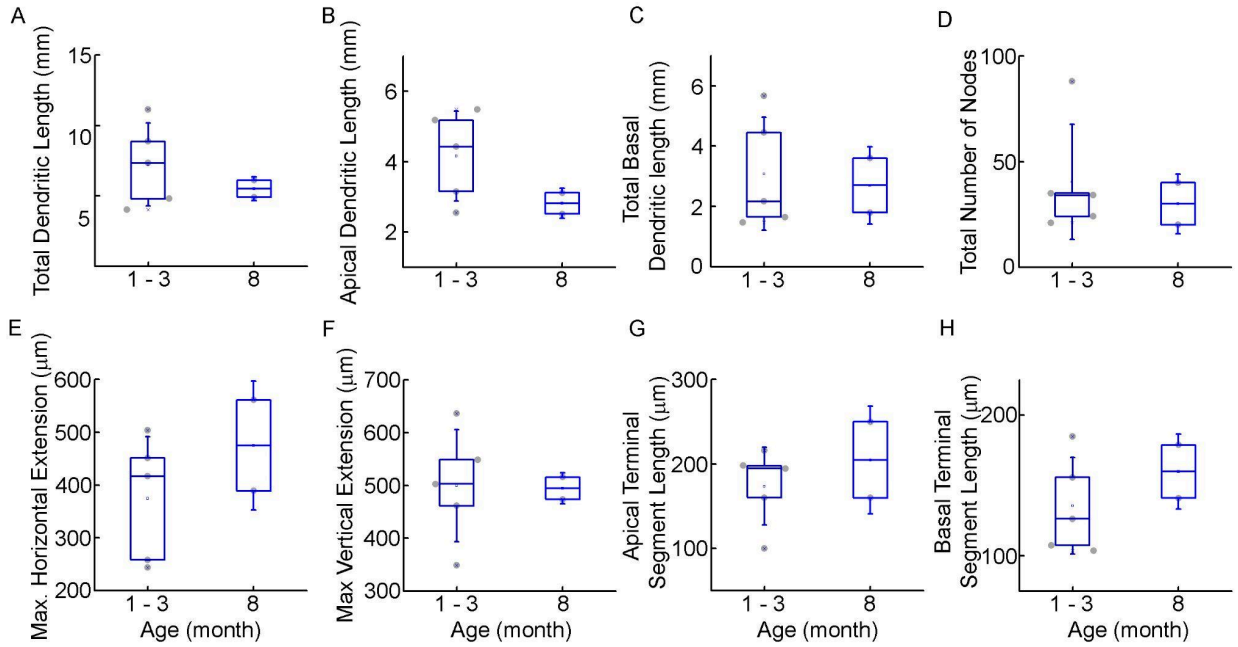


Supplementary Figure 11. Morphological comparison of the examined infant cells.
A-H: Boxplots show morphological features: total (A), apical (B), total basal (C) dendritic length, total number of nodes (D), maximal horizontal (E), and vertical (F) extension, average apical (G) and basal (H) terminal dendritic segment from infant patient during the first and second half of the first year of life.

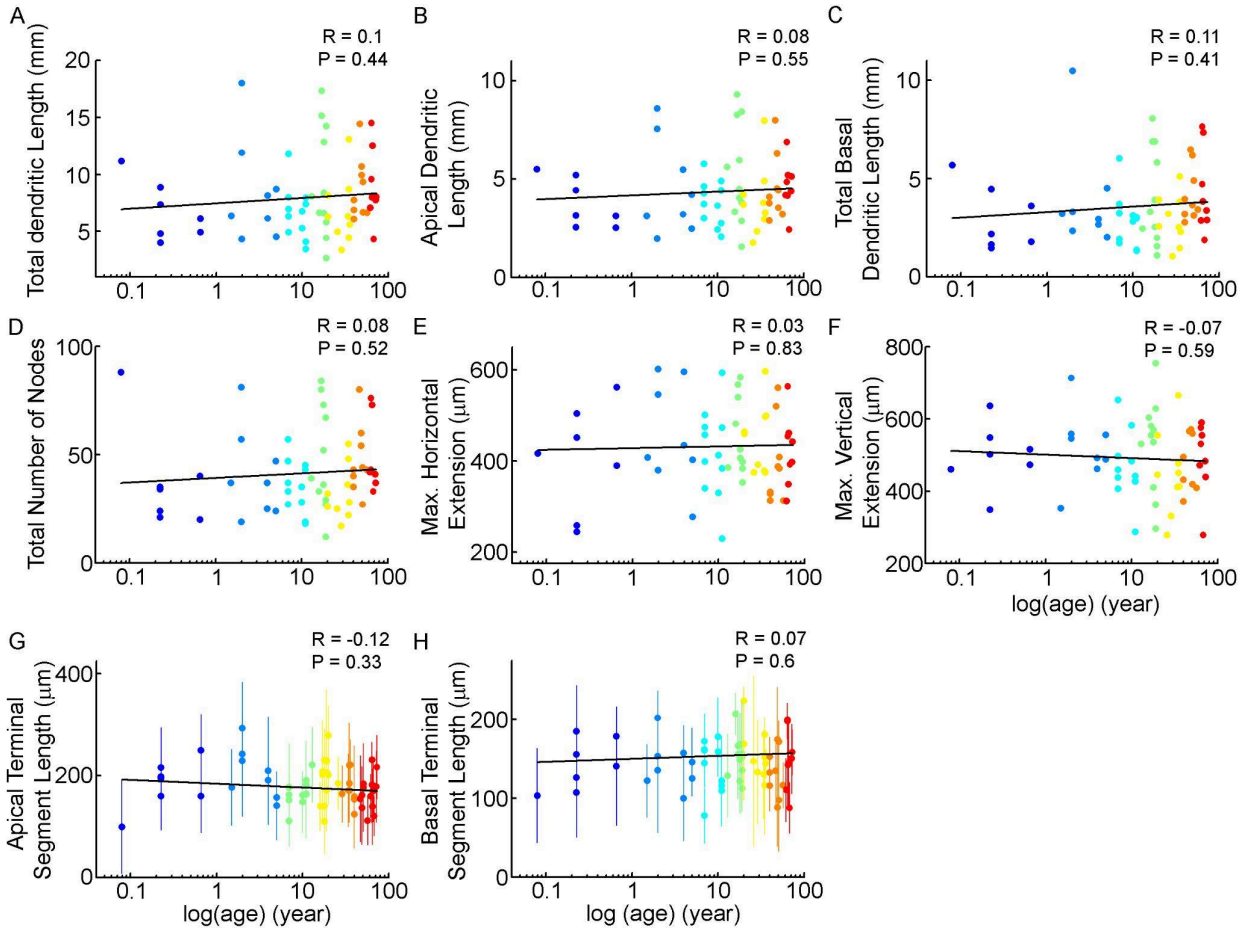


Supplementary Figure 12. Distribution of morphological features with age

A-F: Scatterplots show the distribution of total (A), apical (B), total basal dendritic length (C), total number of bifurcations (D), maximum horizontal extension (E), maximum vertical extension of the dendritic arborisation (F). The age is represented in years on a logarithmic scale.

G-H: Scatterplots show the average apical (G) and basal (H) terminal segment length of the cells, dots indicate the mean segment length of cells, vertical lines show the standard deviation.

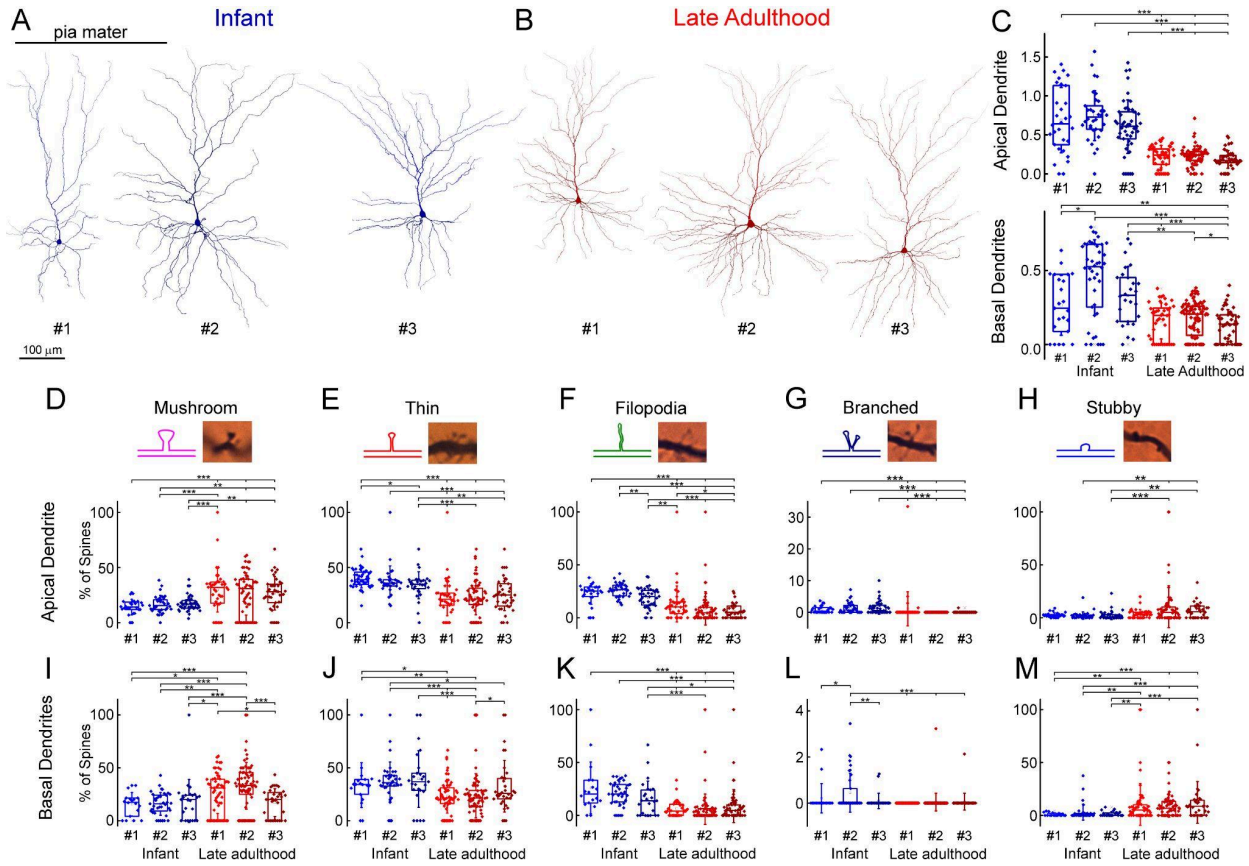


Supplementary Figure 13.

(A) Anatomical 3D reconstructions of the examined n = 3 human L2/3 pyramidal cells from the infant age group.

(B) Anatomical reconstructions (n = 3) from the late adulthood group.

(C) Boxplots showing the spine density on the six individual cells, the infant pyramidal cell shown with blue, the late adulthood pyramidal cell with red (cells are numbered according to figure A, B), on the apical (top) and the basal (bottom) dendrites. Asterisks indicate significance (* $P < 0.05$, ** $P < 0.01$, *** $P < 0.001$, Kruskal-Wallis test with post-hoc Dunn test).

(D-H) The plots show the distribution of mushroom (D), thin (E), filopodium (F), branched (G), and stubby (H) dendritic spine types on the apical dendrites of the reconstructed infant (n = 3, blue) and late adult (n = 3, red) pyramidal cells. Top, schematic illustration and representative images representation of the examined dendritic spine types. Bottom, spine distributions on the individual cells that were examined. Asterisks indicate significance (* $P < 0.05$, ** $P < 0.01$, *** $P < 0.001$, Kruskal-Wallis test with post-hoc Dunn test).

(I-M) Same as D-H but on basal dendrites.

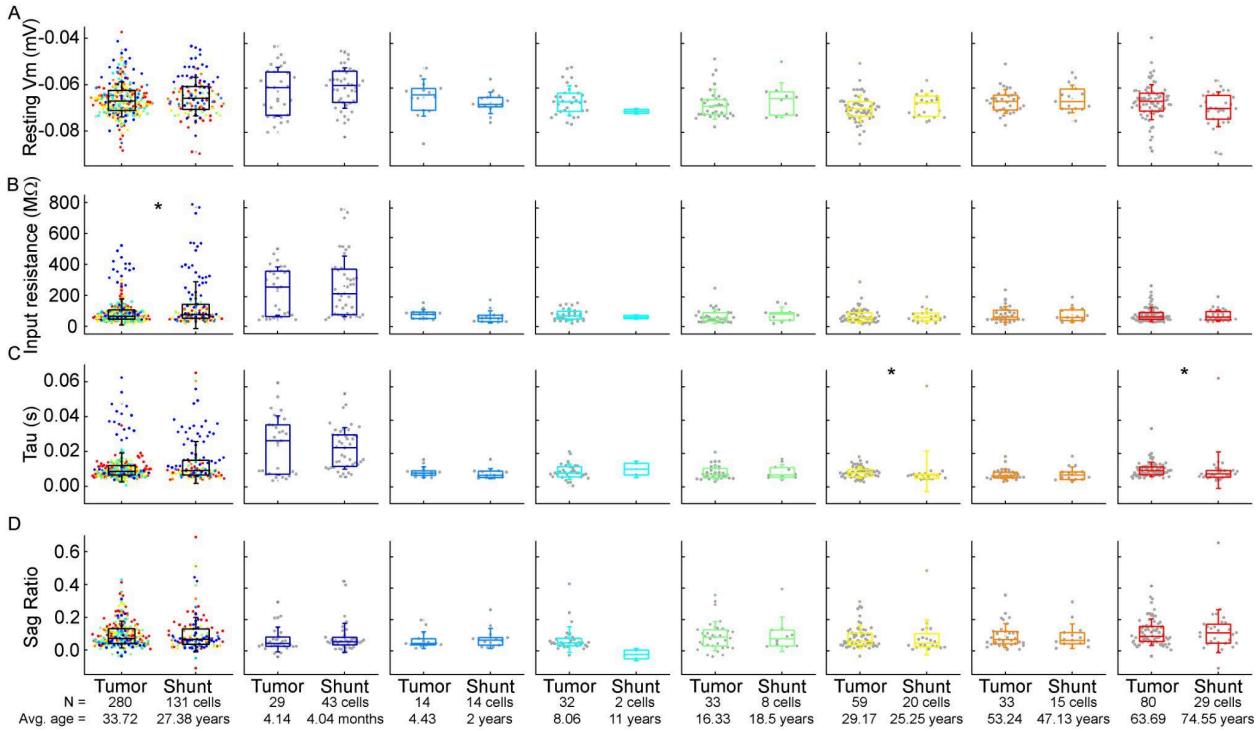


Supplementary Figure 14. Comparison of subthreshold electrophysiological properties of the examined cells from patients with tumor removal or VP shunt surgical procedures.
A-D: Box plots show resting membrane potential (A), input resistance (B), tau (C), and sag ratio (D) from patients with tumor removal (tumor) or VP shunt (shunt) surgical procedures. From left to right: data from all age groups, infant, early childhood, late childhood, adolescence, young adulthood, middle adulthood and late adulthood groups. Asterisks indicate significance (* $P < 0.05$, Mann-Whitney test).

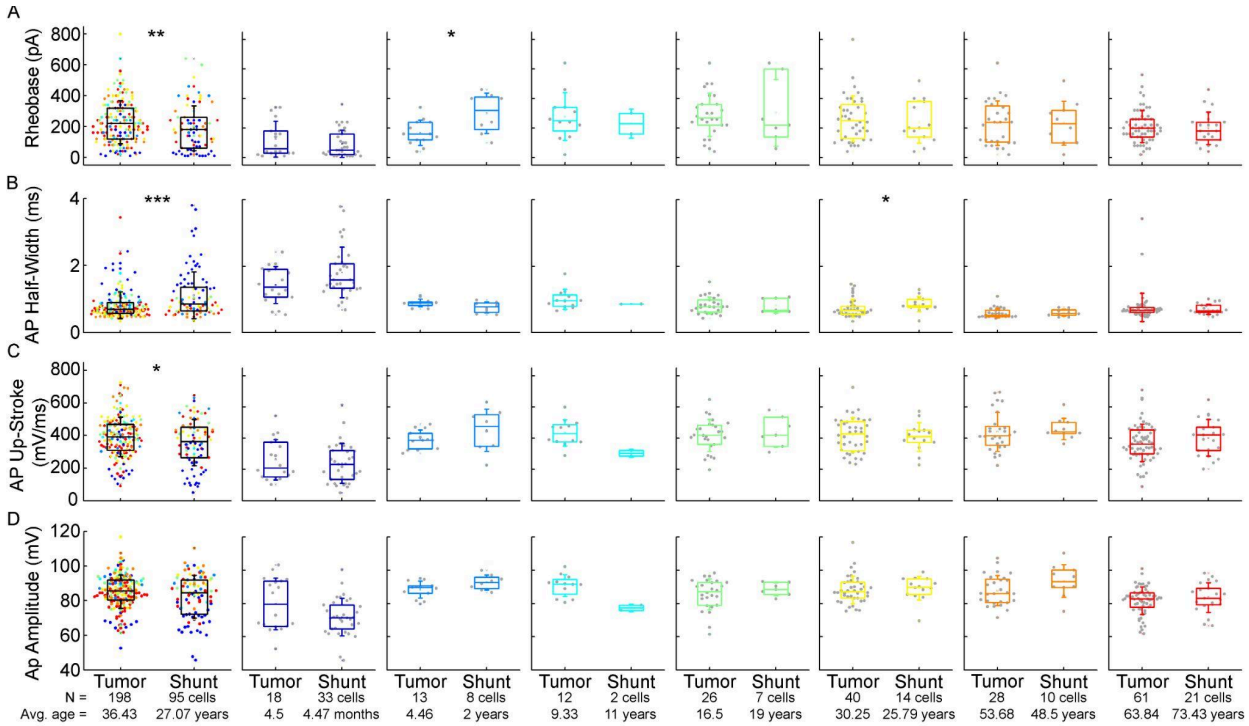


Supplementary Figure 15. Comparison of action potential properties of the examined cells from patients with tumor removal or VP shunt surgical procedures.

A-D: Boxplots show rheobase (A), action potential half-width mean (B), action potential up-stroke (C) and action potential amplitude (D) from patients with tumor removal (tumor) or VP shunt (shunt) surgical procedures. From left to right: data from all age groups, infant, early childhood, late childhood, adolescence, young adulthood, middle adulthood and late adulthood groups. Asterisks indicate significance (* $P < 0.05$, ** $P < 0.01$, *** $P < 0.001$, Mann-Whitney test).

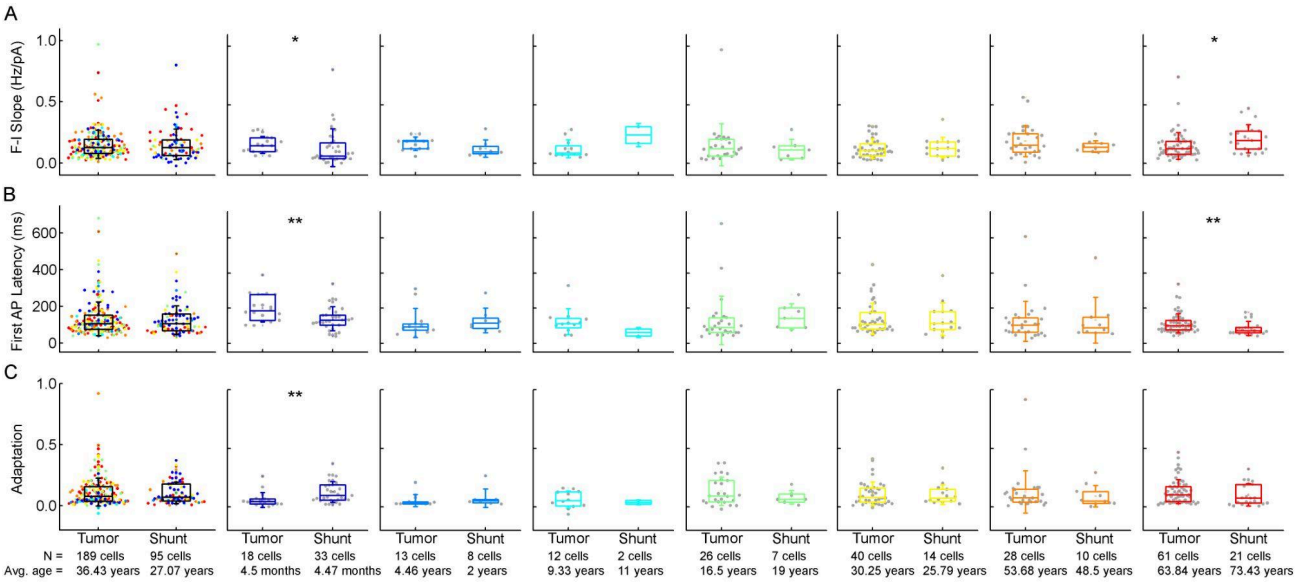


Supplementary Figure 16. Comparison of firing pattern characteristics of the examined cells from patients with tumor removal or VP shunt surgical procedures.
A-C: Box plots showing: F-I slope (A), first AP latency (B), and adaptation of APs (C) from patients with tumor removal (tumor) or VP shunt (shunt) surgical procedures. From left to right: data from all age groups, infant, early childhood, late childhood, adolescence, young adulthood, middle adulthood and late adulthood groups. Asterisks indicate significance (* $P < 0.05$, ** $P < 0.01$, Mann-Whitney test).

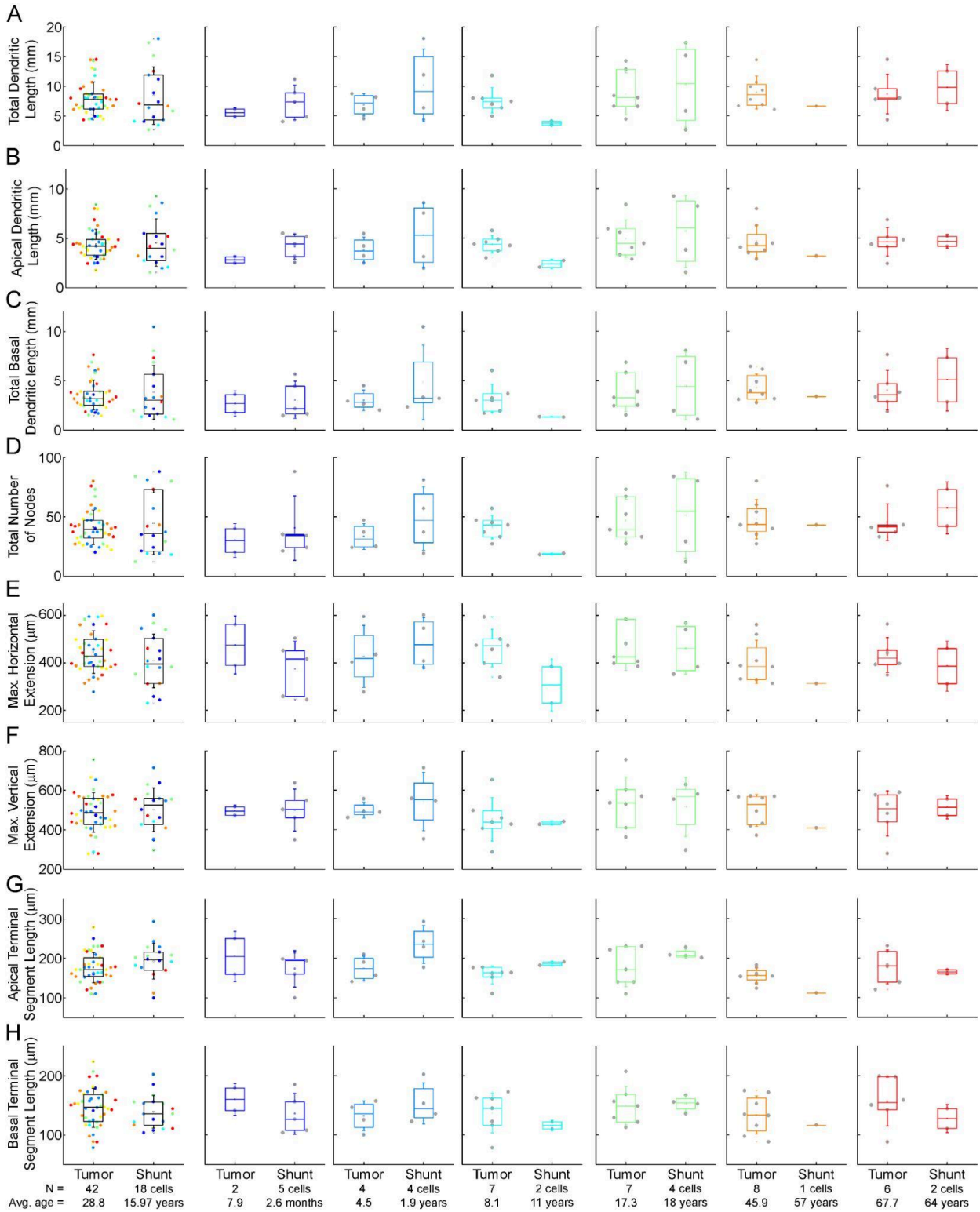


Supplementary Figure 17. Morphological comparison of the examined cells from patients with tumor removal or VP shunt surgical procedures.

A-H: Boxplots showing morphological features: total (A), apical (B), total basal (C), dendritic length, total number of nodes (D), maximal horizontal (E), and vertical (F) extension, average

apical (G) and basal (H) terminal dendritic segment from patients with tumor removal (tumor) or VP shunt (shunt) surgical procedures. From left to right: data from all age groups, infant, early childhood, late childhood, adolescence, middle adulthood and late adulthood groups. Asterisks indicate significance (* P < 0.05, Mann-Whitney test).

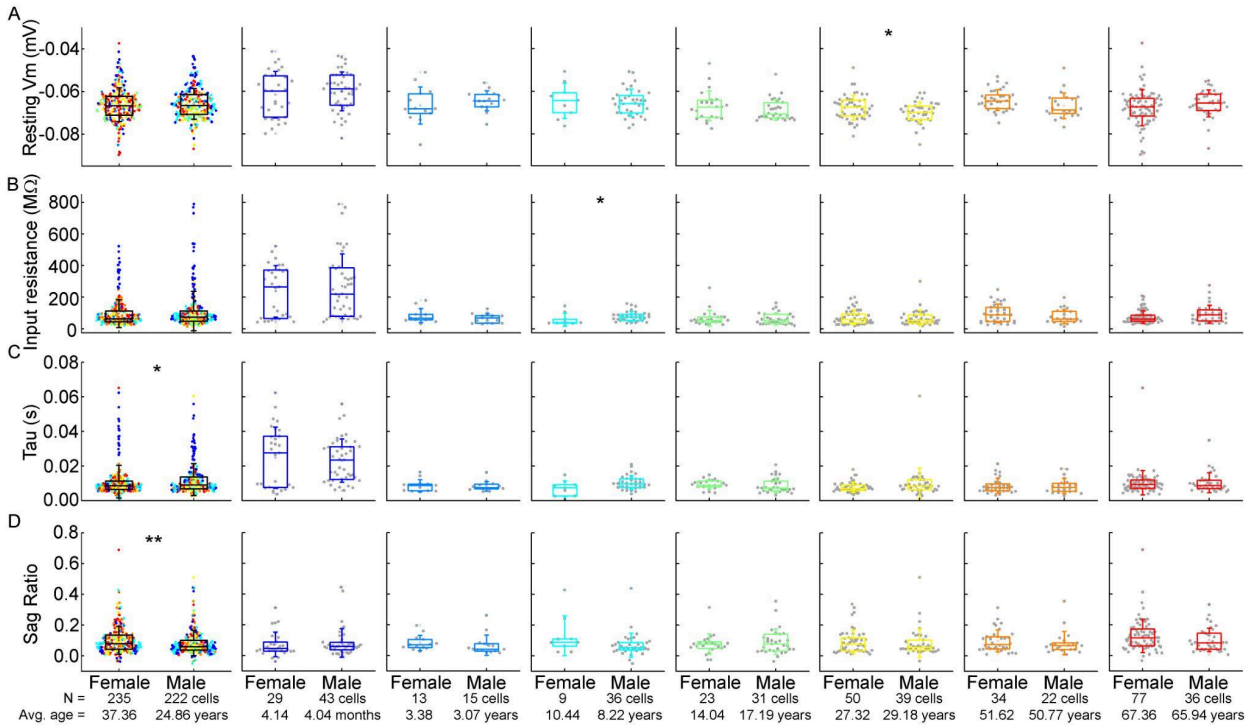


Supplementary Figure 18. Comparison of subthreshold electrophysiological properties of the examined cells from female and male patients.

A-D: Box plots show resting membrane potential (A), input resistance (B), tau (C), and sag ratio (D) from female and male patients. From left to right: data from all age groups, infant, early childhood, late childhood, adolescence, young adulthood, middle adulthood and late adulthood groups. Asterisks indicate significance (* P < 0.05, ** P < 0.01 Mann-Whitney test or two sample t-test).

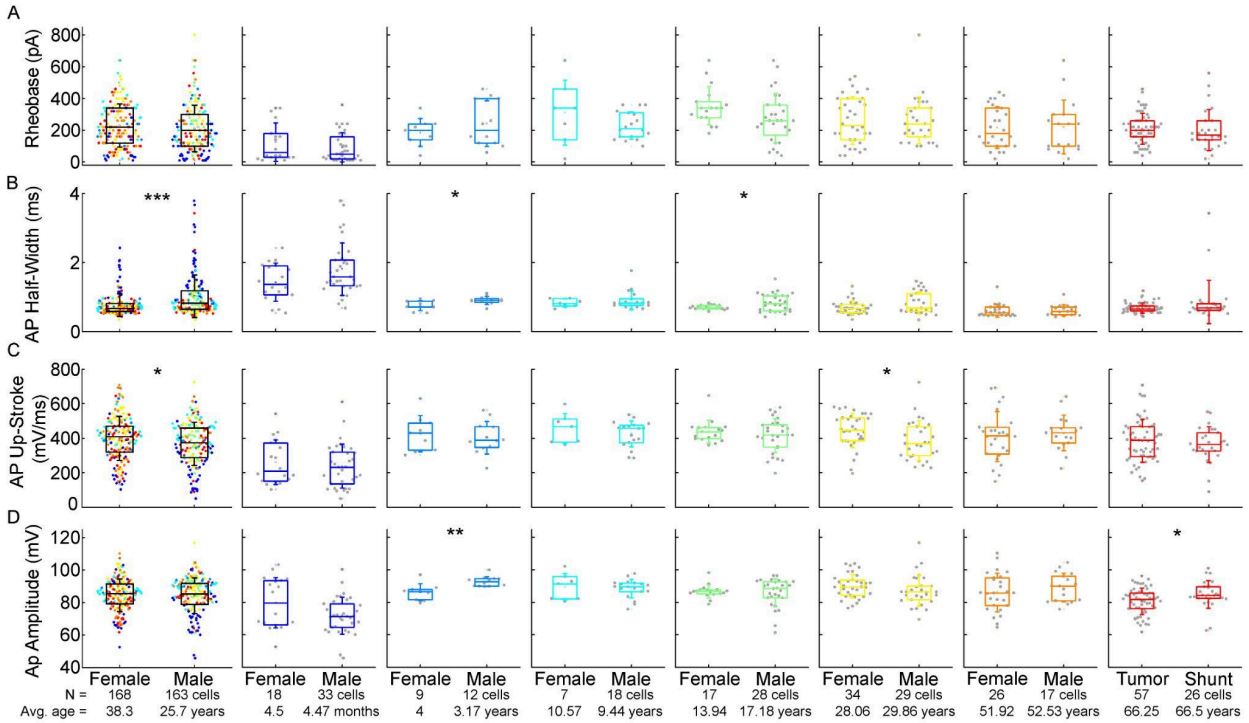


Supplementary Figure 19. Comparison of action potential properties of the examined cells from female and male patients.

A-D: Boxplots show rheobase (A), action potential half-width mean (B), action potential up-stroke (C) and action potential amplitude (D) from female and male patients. From left to right: data from all age groups, infant, early childhood, late childhood, adolescence, young adulthood, middle adulthood and late adulthood groups. Asterisks indicate significance (* P < 0.05, ** P < 0.01, *** P < 0.001, Mann-Whitney test or two sample t-test).

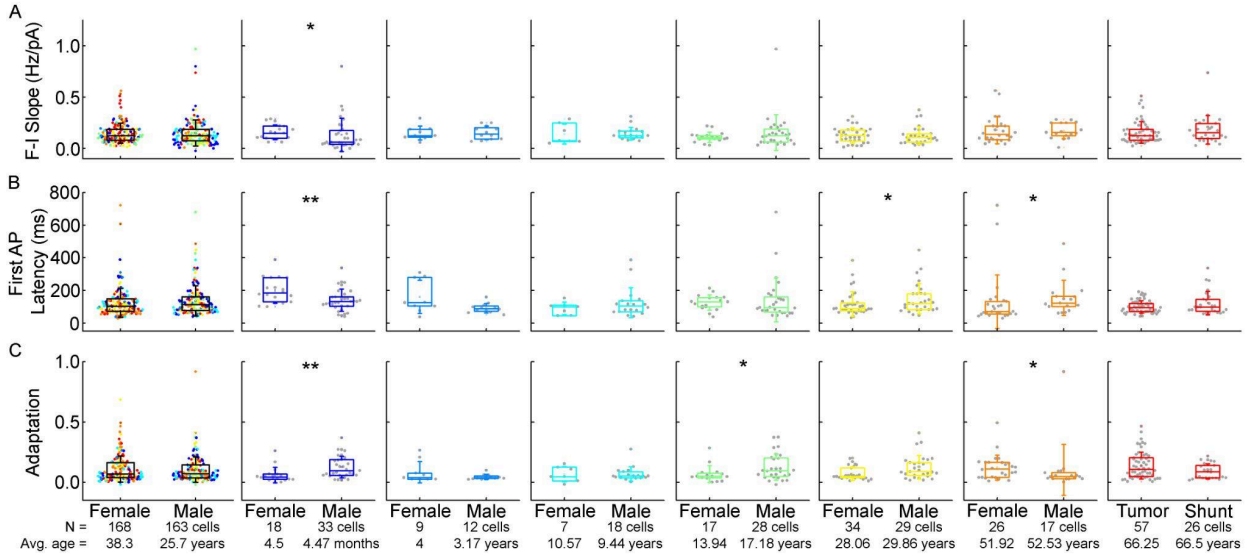


Supplementary Figure 20. Comparison of firing pattern characteristics of the examined cells from female and male patients.

A-C: Box plots showing: F-I slope (A), first AP latency (B), and adaptation of APs (C) from female and male patients. From left to right: data from all age groups, infant, early childhood, late childhood, adolescence, young adulthood, middle adulthood, and late adulthood groups. Asterisks indicate significance (* P < 0.05, ** P < 0.01, Mann-Whitney test or two sample t-test).

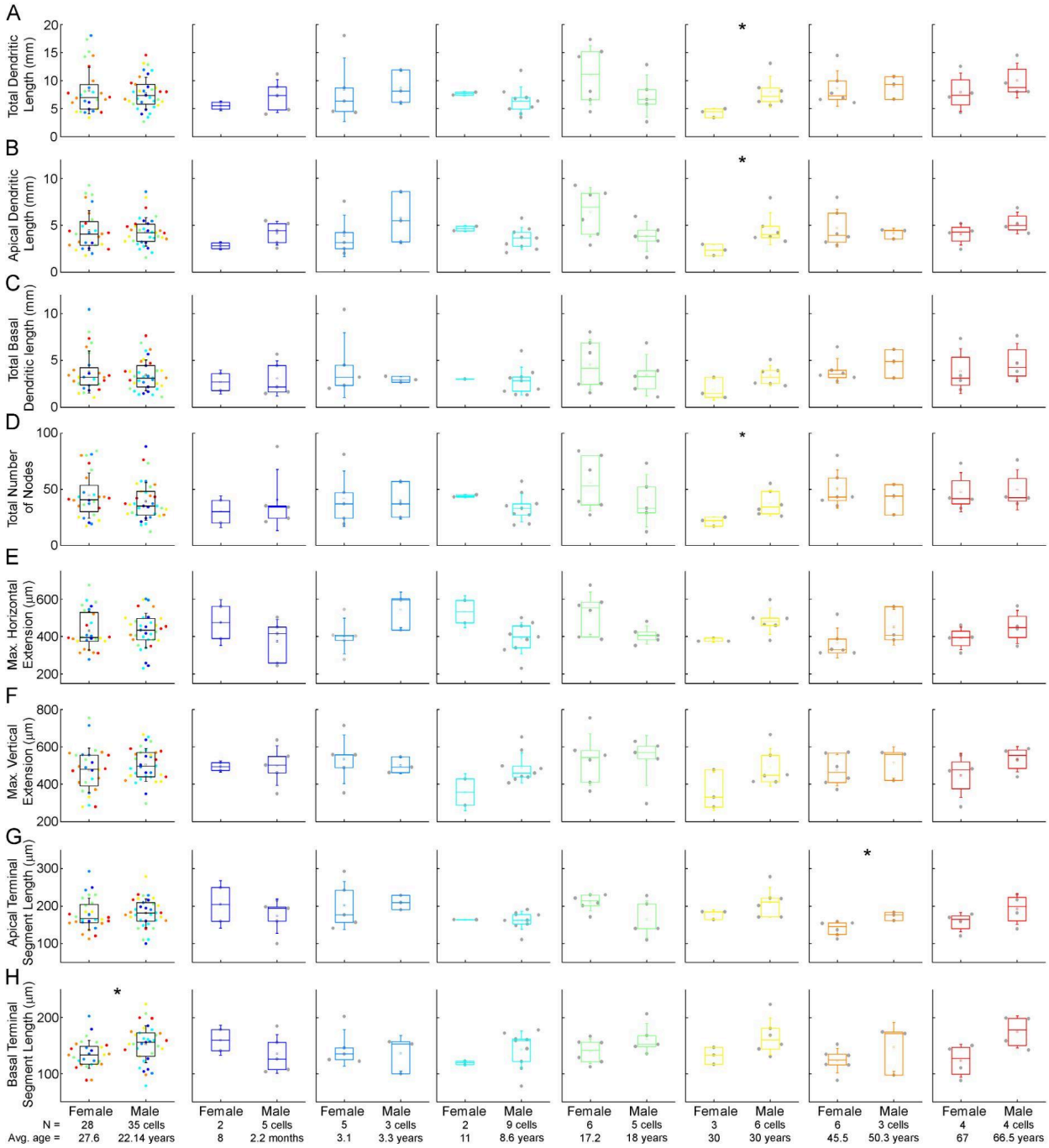


Supplementary Figure 21. Morphological comparison of the examined cells from female and male patients.

A-H: Boxplots showing morphological features: total (A), apical (B), total basal (C), dendritic length, total number of nodes (D), maximal horizontal (E), and vertical (F) extension, average

apical (G) and basal (H) terminal dendritic segment from female and male patients. From left to right: data from all age groups, infant, early childhood, late childhood, adolescence and late adulthood groups.

## References


Aller, M. I. & Wisden, W. Changes in expression of some two-pore domain potassium channel genes (KCNK) in selected brain regions of developing mice. Neuroscience 151, 1154–1172 (2008).

Beaulieu-Laroche L, Toloza EHS, van der Goes MS, Lafourcade M, Barnagian D, Williams ZM, Eskandar EN, Frosch MP, Cash SS, Harnett MT. Enhanced Dendritic Compartmentalization in Human Cortical Neurons. Cell. 2018 Oct 18;175(3):643-651.e14. doi: 10.1016/j.cell.2018.08.045. PMID: 30340039; PMCID: PMC6197488

Beck D, de Lange AG, Maximov II, Richard G, Andreassen OA, Nordvik JE, Westlye LT. White matter microstructure across the adult lifespan: A mixed longitudinal and cross-sectional study using advanced diffusion models and brain-age prediction. Neuroimage. 2021 Jan 1;224:117441. doi: 10.1016/j.neuroimage.2020.117441.

Benavides-Piccione R, Fernaud-Espinosa I, Robles V, Yuste R, DeFelipe J. Age-based comparison of human dendritic spine structure using complete three-dimensional reconstructions. Cereb Cortex. 2013 Aug;23(8):1798-810. doi: 10.1093/cercor/bhs154.

Berg, J., Sorensen, S.A., Ting, J.T. et al. Human neocortical expansion involves glutamatergic neuron diversification. Nature 598, 151–158 (2021). https://doi.org/10.1038/s41586-021-03813-8

Bethlehem RAI et al., Brain charts for the human lifespan. Nature volume 604, pages 525–533 (2022) doi: 10.1038/s41586-022-04554-y https://doi.org/10.1038/s41586-022-04554-y

Bourne JN, Harris KM. Balancing structure and function at hippocampal dendritic spines. Annu Rev Neurosci. 2008;31:47-67. doi:10.1146/annurev.neuro.31.060407.125646.

Chang YM, Rosene DL, Killiany RJ, Mangiamele LA, Luebke JI. Increased action potential firing rates of layer 2/3 pyramidal cells in the prefrontal cortex are significantly related to cognitive performance in aged monkeys. Cereb Cortex. 2005 Apr;15(4):409-18. doi: 10.1093/cercor/bhh144.

Connors BW. Intrinsic neuronal physiology and the functions, dysfunctions and development of neocortex. Prog Brain Res 102: 195-203, 1994.

Coskren PJ, Luebke JI, Kabaso D, Wearne SL, Yadav A, Rumbell T, Hof PR, Weaver CM. Functional consequences of age-related morphologic changes to pyramidal neurons of the rhesus monkey prefrontal cortex. J Comput Neurosci. 2015 Apr;38(2):263-83. doi: 10.1007/s10827-014-0541-5.

Craik FI, Bialystok E. Cognition through the lifespan: mechanisms of change. Trends Cogn Sci. 2006 Mar;10(3):131-8. doi: 10.1016/j.tics.2006.01.007. Epub 2006 Feb 7

Doischer D, Hosp JA, Yanagawa Y, Obata K, Jonas P, Vida I, Bartos M. Postnatal differentiation of basket cells from slow to fast signaling devices. J Neurosci. 2008 Nov 26;28(48):12956-68. doi: 10.1523/JNEUROSCI.2890-08.2008.

Dumitriu D, Hao J, Hara Y, Kaufmann J, Janssen WG, Lou W, Rapp PR, Morrison JH. Selective changes in thin spine density and morphology in monkey prefrontal cortex correlate with aging-related cognitive impairment. J Neurosci. 2010 Jun 2;30(22):7507-15. doi: 10.1523/JNEUROSCI.6410-09.2010.

Elston GN & Fujita I, Pyramidal cell development: postnatal spinogenesis, dendritic growth, axon growth, and electrophysiology. Front Neuroanat. 2014; 8: 78. doi: 10.3389/fnana.2014.00078

Erraji-Benchekroun L, Underwood MD, Arango V, Galfalvy H, Pavlidis P, Smyrniotopoulos P, Mann JJ, Sibille E. Molecular aging in human prefrontal cortex is selective and continuous throughout adult life. Biological Psychiatry Volume 57, Issue 5, 1 March 2005, Pages 549-558, https://doi.org/10.1016/j.biopsych.2004.10.034

Etherington SJ., Williams SR., Postnatal Development of Intrinsic and Synaptic Properties Transforms Signaling in the Layer 5 Excitatory Neural Network of the Visual Cortex. Journal of Neuroscience 29 June 2011, 31 (26) 9526-9537; DOI: 10.1523/JNEUROSCI.0458-11.2011

Eyal G., Mansvelder HD., de Kock CPJ., Segev I. Dendrites Impact the Encoding Capabilities of the Axon. Journal of Neuroscience 11 June 2014, 34 (24) 8063-8071; DOI: 10.1523/JNEUROSCI.5431-13.2014

Globus, A., Rosenzweig, M. R., Bennett, E. L., & Diamond, M. C. (1973). Effects of differential experience on dendritic spine counts in rat cerebral cortex. Journal of Comparative and Physiological Psychology, 82(2), 175–181. https://doi.org/10.1037/h0033910

Goldstein, SAN., Bockenhauer, D., O'Kelly, I., Zilberberg, N. Potassium leak channels and the KCNK family of two-p-domain subunits. Nat. Rev. Neurosci. 2, 175–184 (2001)

Greenough, WT., Volkmar, FR. Pattern of dendritic branching in occipital cortex of rats reared in complex environments. Experimental Neurology, Volume 40, Issue 2, August 1973, Pages 491-504 https://doi.org/10.1016/0014-4886(73)90090-3

Guet-McCreight A. , Chameh H.M., Mahallati S., Wishart M., Tripathy S.J., Valiante T.A., Hay E. (2023) Age-dependent increased sag amplitude in human pyramidal neurons dampens baseline cortical activity. Cerebral Cortex, Volume 33, Issue 8, 15 April 2023, Pages 4360–4373, https://doi.org/10.1093/cercor/bhac348

Holloway Jr. R L. Dendritic branching: some preliminary results of training and complexity in rat visual cortex. Brain Research Volume 2, Issue 4, October 1966, Pages 393-396 https://doi.org/10.1016/0006-8993(66)90009-6

Horibe S, Tarusawa E, Komatsu Y, Yoshimura Y, Ni2+-sensitive T-type Ca2+ channel currents are regulated in parallel with synaptic and visual response plasticity in visual cortex, Neuroscience Research, Volume 87, 2014, Pages 33-39, ISSN 0168-0102, https://doi.org/10.1016/j.neures.2014.07.001.

Huguenard JR, Hamill OP, Prince DA. Developmental changes in Na+ conductances in rat neocortical neurons: appearance of a slowly inactivating component. J Neurophysiol. 1988 Mar;59(3):778-95. doi: 10.1152/jn.1988.59.3.778. PMID: 2452862.

Huttenlocher PR (1979) Synaptic density in human frontal cortex — Developmental changes and effects of aging. Brain Res 163:195–205 Available at: http://linkinghub.elsevier.com/retrieve/pii/0006899379903494.

Huttenlocher PR, Dabholkar AS. Regional differences in synaptogenesis in human cerebral cortex. J Comp Neurol. 1997 Oct 20;387(2):167-78. doi:10.1002/(sici)1096-9861(19971020)387:2<167::aid-cne1>3.0.co;2-z. PMID: 9336221.

Huttenlocher PR, de Courten C, Garey LJ, Van der Loos H (1982) Synaptogenesis in human visual cortex — evidence for synapse elimination during normal development. Neurosci Lett 33:247–252 Available at: https://linkinghub.elsevier.com/retrieve/pii/0304394082903792.

Jacobs B, Driscoll L, Schall M, Life-Span Dendritic and Spine Changes in Areas 10 and 18 of Human Cortex: A Quantitative Golgi Study. THE JOURNAL OF COMPARATIVE NEUROLOGY 386:661–680 (1997)

Kalmbach BE., et al. h-Channels Contribute to Divergent Intrinsic Membrane Properties of Supragranular Pyramidal Neurons in Human versus Mouse Cerebral Cortex. Neuron Volume 100, Issue 5, 5 December 2018, Pages 1194-1208.e5 https://doi.org/10.1016/j.neuron.2018.10.012

Kang, H., Kawasawa, Y., Cheng, F. et al. Spatio-temporal transcriptome of the human brain. Nature 478, 483–489 (2011). https://doi.org/10.1038/nature10523

Kasper, E.M., Larkman, A.U., Lübke, J. and Blakemore, C. (1994), Pyramidal neurons in layer 5 of the rat visual cortex. II. Development of electrophysiological properties. J. Comp. Neurol., 339: 475-494. https://doi.org/10.1002/cne.903390403

Kastellakis, G., Tasciotti, S., Pandi, I., Poirazi, P. The dendritic engram. Front. Behav. Neurosci., 27 July 2023 Sec. Learning and Memory, Volume 17 - 2023 | https://doi.org/10.3389/fnbeh.2023.1212139

Kelly AM, Di Martino A, Uddin LQ, Shehzad Z, Gee DG, Reiss PT, Margulies DS, Castellanos FX, Milham MP. Development of anterior cingulate functional connectivity from late childhood to early adulthood. Cereb Cortex. 2009 Mar;19(3):640-57. doi: 10.1093/cercor/bhn117.

Koenderink MJTh, Uylings HBM. Postnatal maturation of layer V pyramidal neurons in the human prefrontal cortex. A quantitative Golgi analysis. Brain Research Volume 678, Issues 1–2, 24 April 1995, Pages 233-243, https://doi.org/10.1016/0006-8993(95)00206-6

Kroon T, van Hugte E, van Linge L, Mansvelder HD & Meredith RM, Early postnatal development of pyramidal neurons across layers of the mouse medial prefrontal cortex. Scientific Reports 9:5037. doi: 10.1038/s41598-019-41661-9

Kuzawa CW, Chugani HT, Grossman LI, Lipovich L, Muzik O, Hof PR, Wildman DE, Sherwood CC, Leonard WR, Lange N. Metabolic costs and evolutionary implications of human brain development. Proc Natl Acad Sci U S A. 2014 Sep 9;111(36):13010-5. doi: 10.1073/pnas.1323099111. Epub 2014 Aug 25.

Li BZ, Sumera A, Booker SA, McCullagh EA. Current Best Practices for Analysis of Dendritic Spine Morphology and Number in Neurodevelopmental Disorder Research. ACS Chem Neurosci. 2023 May 3;14(9):1561-1572. doi: 10.1021/acschemneuro.3c00062. Epub 2023 Apr 18.

Linaro D, Vermaercke B, Iwata R, Ramaswamy A, Libé-Philippot B, Boubakar L, Davis BA, Wierda K, Davie K, Poovathingal S, Penttila PA, Bilheu A, De Bruyne L, Gall D,Conzelmann KK,Bonin V, Vanderhaeghen P. Xenotransplanted Human Cortical Neurons Reveal Species-Specific Development and Functional Integration into Mouse Visual Circuits. Volume 104, Issue 5, 4 December 2019, Pages 972-986.e6, https://doi.org/10.1016/j.neuron.2019.10.002

Luebke JI, Chang YM. Effects of aging on the electrophysiological properties of layer 5 pyramidal cells in the monkey prefrontal cortex. Neuroscience. 2007 Dec 12;150(3):556-62. doi: 10.1016/j.neuroscience.2007.09.042.

Luebke JI, Medalla M, Amatrudo JM, Weaver CM, Crimins JL, Hunt B, Hof PR, Peters A. Age-related changes to layer 3 pyramidal cells in the rhesus monkey visual cortex. Cereb Cortex. 2015 Jun;25(6):1454-68. doi: 10.1093/cercor/bht336. Epub 2013 Dec 8.

Luhmann HJ., Reiprich RA, Hanganu I, Kilb W, Cellular physiology of the neonatal rat cerebral cortex: Intrinsic membrane properties, sodium and calcium currents. (2000) Journal of Neuroscience ResearchVolume 62, Issue 4, https://doi.org/10.1002/1097-4547(20001115)62:4

Luna B, Marek S, Larsen B, Tervo-Clemmens B, Chahal R. An integrative model of the maturation of cognitive control. Annu Rev Neurosci. 2015 Jul 8;38:151-70. doi: 10.1146/annurev-neuro-071714-034054.

Mainen, Z., Sejnowski, T. Influence of dendritic structure on firing pattern in model neocortical neurons. Nature 382, 363–366 (1996). https://doi.org/10.1038/382363a0

Matsuzaki M, Ellis-Davies GC, Nemoto T, Miyashita Y, Iino M, Kasai H. Dendritic spine geometry is critical for AMPA receptor expression in hippocampal CA1 pyramidal neurons. Nat Neurosci. 2001 Nov;4(11):1086-92. doi: 10.1038/nn736.

Mavroudis IA, Manani MG, Petrides F, Dados D, Ciobica A, Padurariu M, Petsoglou K, Njau SN, Costa VG, Baloyannis SJ. Age-related dendritic and spinal alterations of pyramidal cells of the human visual cortex. Folia Neuropathol 2015; 53 (2): 100-110. DOI: 10.5114/fn.2015.52406

McAllister AK. Cellular and molecular mechanisms of dendrite growth. Cereb Cortex. 2000 Oct;10(10):963-73. doi: 10.1093/cercor/10.10.963. PMID: 11007547.

McCormick, D A, Prince, D A, (1987), Post-natal development of electrophysiological properties of rat cerebral cortical pyramidal neurones. The Journal of Physiology, 393 doi: 10.1113/jphysiol.1987.sp016851.

Michael L. Molineux, Fernando R. Fernandez, W. Hamish Mehaffey, Ray W. Turner. A-Type and T-Type Currents Interact to Produce a Novel Spike Latency-Voltage Relationship in Cerebellar Stellate Cells.Journal of Neuroscience 23 November 2005, 25 (47) 10863-10873; DOI: 10.1523/JNEUROSCI.3436-05.2005

Molnár Z, Luhmann HJ, Kanold PO. Transient cortical circuits match spontaneous and sensory-driven activity during development. Science. 2020 Oct 16;370(6514):eabb2153. doi: 10.1126/science.abb2153.

Moore, T.L., Medalla, M., Ibañez, S. et al. Neuronal properties of pyramidal cells in lateral prefrontal cortex of the aging rhesus monkey brain are associated with performance deficits on spatial working memory but not executive function. GeroScience 45, 1317–1342 (2023).

Moradi Chameh H, Rich S, Wang L, Chen F-D, Zhang L, Carlen PL, Tripathy SJ, Valiante TA (2021) Diversity amongst human cortical pyramidal neurons revealed via their sag currents and frequency preferences. Nat Commun 12:2497

Mrzljak L, Uylings HB, Van Eden CG, Judás M. Neuronal development in human prefrontal cortex in prenatal and postnatal stages. Prog Brain Res. 1990;85:185-222. doi: 10.1016/s0079-6123(08)62681-3.

Nusser Z, Lujan R, Laube G, Roberts JD, Molnar E, Somogyi P. Cell type and pathway dependence of synaptic AMPA receptor number and variability in the hippocampus. Neuron. 1998 Sep;21(3):545-59. doi: 10.1016/s0896-6273(00)80565-6.

Oláh G, Lákovics R, Shapira S,Leibner Y, Szűcs A, Csajbók ÉA, Barzó P, Molnár G, Segev I, Tamás G. 2024 Accelerated signal propagation speed in human neocortical microcircuits.eLife13:RP93781 https://doi.org/10.7554/eLife.93781.1

Oswald AM, Reyes AD. Development of inhibitory timescales in auditory cortex. Cereb Cortex. 2011 Jun;21(6):1351-61. doi: 10.1093/cercor/bhq214.

Perez-García, P., Pardillo-Díaz. R.,Geribaldi-Doldán, N., Gómez-Oliva, R., Domínguez-García, S., Castro, C., Nunez-Abades, P.,Carrascal, L. Refinement of Active and Passive Membrane Properties of Layer V Pyramidal Neurons in Rat Primary Motor Cortex During Postnatal Development. Front. Mol. Neurosci., 01 December 2021 Sec. Neuroplasticity and Development, Volume 14 - 2021 | https://doi.org/10.3389/fnmol.2021.754393

Petanjek Z, Judaš M, Kostović I, Uylings HBM, Lifespan Alterations of Basal Dendritic Trees of Pyramidal Neurons in the Human Prefrontal Cortex: A Layer-Specific Pattern, Cerebral Cortex, Volume 18, Issue 4, April 2008, Pages 915–929, https://doi.org/10.1093/cercor/bhm124

Petanjek, Z. et al. Extraordinary neoteny of synaptic spines in the human prefrontal cortex. Proc. Natl Acad. Sci. USA 108, 13281–13286 (2011). Quantitative assessment of dendritic spine density demonstrates striking neoteny of synaptic development characterizing human cortex development.

Petanjek, Z. et al. The protracted maturation of associative layer IIIC pyramidal neurons in the human prefrontal cortex during childhood: a major role in cognitive development and selective alteration in autism. Front. Psychiatry 10, 122 (2019)

Peters R, Ageing and the brain. Postgraduate Medical Journal, Volume 82, Issue 964, February 2006, Pages 84–88, https://doi.org/10.1136/pgmj.2005.036665

Picken Bahrey, H. L. & Moody, W. J. Early Development of Voltage-Gated Ion Currents and Firing Properties in Neurons of the Mouse Cerebral Cortex. J. Neurophysiol. 89, 1761–1773 (2003)

Popescu IR, Le KQ, Ducote AL, Li JE, Leland AE, Mostany R. Increased intrinsic excitability and decreased synaptic inhibition in aged somatosensory cortex pyramidal neurons.Neurobiology of Aging Volume 98, February 2021, Pages 88-98, https://doi.org/10.1016/j.neurobiolaging.2020.10.007

Rakic, P Evolution of the neocortex: a perspective from developmental biology. Nat Rev Neurosci. 2009 Oct;10(10):724-35. doi: 10.1038/nrn2719.

Stiles J, Jernigan TL. The basics of brain development. Neuropsychol Rev. 2010 Dec;20(4):327-48. doi: 10.1007/s11065-010-9148-4. Epub 2010 Nov 3. PMID: 21042938; PMCID: PMC2989000.

Tau, G., Peterson, B. Normal Development of Brain Circuits. Neuropsychopharmacol 35, 147–168 (2010). https://doi.org/10.1038/npp.2009.115

van Blooijs D, van den Boom MA, van der Aar JF, Huiskamp GM, Castegnaro G, Demuru M, Zweiphenning WJEM, van Eijsden P, Miller KJ, Leijten FSS, Hermes D. Developmental trajectory of transmission speed in the human brain. Nat Neurosci. 2023 Apr;26(4):537-541. doi: 10.1038/s41593-023-01272-0.

van Elburg RAJ, van Ooyen A (2010) Impact of Dendritic Size and Dendritic Topology on Burst Firing in Pyramidal Cells. PLoS Comput Biol 6(5): e1000781. https://doi.org/10.1371/journal.pcbi.1000781
Vardalaki, D., Chung, K. & Harnett, M.T. Filopodia are a structural substrate for silent synapses in adult neocortex. Nature 612, 323–327 (2022). https://doi.org/10.1038/s41586-022-05483-6

Vetter P, Roth A, Häusser M. Propagation of action potentials in dendrites depends on dendritic morphology. J Neurophysiol. 2001 Feb;85(2):926-37. doi: 10.1152/jn.2001.85.2.926. PMID: 11160523.

Wang M, Ramos BP, Paspalas CD, Shu Y, Simen A, Duque A, Vijayraghavan S, Brennan A, Dudley A, Nou E, et al. A2A-adrenoceptors strengthen working memory networks by inhibiting cAMP-HCN channel signaling in prefrontal cortex. Cell. 2007: 129(2): 397–410.

Wang, M., Gamo, N., Yang, Y. et al. Neuronal basis of age-related working memory decline. Nature 476, 210–213 (2011). https://doi.org/10.1038/nature10243

Yeatman JD, Wandell BA, Mezer AA. Lifespan maturation and degeneration of human brain white matter. Nat Commun. 2014 Sep 17;5:4932. doi: 10.1038/ncomms5932.

Yoshimura, Y., Dantzker, J. & Callaway, E. Excitatory cortical neurons form fine-scale functional networks. Nature 433, 868–873 (2005). https://doi.org/10.1038/nature03252

Zhong-wei Zhang Maturation of Layer V Pyramidal Neurons in the Rat Prefrontal Cortex: Intrinsic Properties and Synaptic Function 01 MAR 2004 https://doi.org/10.1152/jn.00855.2003

Zhu, J. J. (2000). Maturation of layer 5 neocortical pyramidal neurons: amplifying salient layer 1 and layer 4 inputs by Ca2+ action potentials in adult rat tuft dendrites. J. Physiol. 526, 571–587. doi: 10.1111/j.1469-7793.2000.00571.x